The Heat Is On: Observations and Trends of Heat Stress Metrics during Florida Summers

CAITLYN MCALLISTER,[a] AARON STEPHENS,[a] AND SHAWN M. MILRAD[a]

[a] *Meteorology Program, Applied Aviation Sciences Department, Embry-Riddle Aeronautical University, Daytona Beach, Florida*

(Manuscript received 11 June 2021, in final form 27 December 2021)

ABSTRACT: Extreme heat is annually the deadliest weather hazard in the United States and is strongly amplified by climate change. In Florida, summer heat waves have increased in frequency and duration, exacerbating negative human health impacts on a state with a substantial older population and industries (e.g., agriculture) that require frequent outdoor work. However, the combined impacts of temperature and humidity (heat stress) have not been previously investigated. For eight Florida cities, this study constructs summer climatologies and trend analyses (1950–2020) of two heat stress metrics: heat index (HI) and wet-bulb globe temperature (WBGT). While both incorporate temperature and humidity, WBGT also includes wind and solar radiation and is a more comprehensive measure of heat stress on the human body. With minor exceptions, results show increases in average summer daily maximum, mean, and minimum HI and WBGT throughout Florida. Daily minimum HI and WBGT exhibit statistically significant increases at all eight stations, emphasizing a hazardous rise in nighttime heat stress. Corresponding to other recent studies, HI and WBGT increases are largest in coastal subtropical locations in central and southern Florida (i.e., Daytona Beach, Tampa, Miami, and Key West) but exhibit no conclusive relationship with urbanization changes. Danger (103°–124°F; 39.4°–51.1°C) HI and high (>88°F; 31.1°C) WBGT summer days exhibit significant frequency increases across the state. Especially at coastal locations in the Florida Peninsula and Keys, danger HI and high WBGT days now account for >20% of total summer days, emphasizing a substantial escalation in heat stress, particularly since 2000.

SIGNIFICANCE STATEMENT: Extreme heat is the deadliest U.S. weather hazard. Although Florida is known for its warm and humid climate, it is not immune from heat stress (combined temperature and humidity) impacts on human health, particularly given its older population and prevalence of outdoor (e.g., agriculture) work. We analyze summer trends in two heat stress metrics at eight Florida cities since 1950. Results show that heat stress is increasing significantly, particularly at coastal locations in central and southern Florida and at night. The number of dangerous heat stress days per summer is also increasing across Florida, especially since 2000. Our analysis emphasizes that despite some acclimation, Florida is still susceptible to a serious escalation in extreme heat as the climate warms.

KEYWORDS: Subtropics; Extreme events; Climate change; Climatology; Humidity; Trends

1. Introduction

Extreme heat, often referred to as the "silent meteorological killer," has seen global and widespread regional increases in frequency, duration, and intensity that are strongly linked to climate change (e.g., Perkins et al. 2012; Perkins 2015; Mora et al. 2017; Keellings and Moradkhani 2020). In the United States, heat is the deadliest annual weather-related hazard (e.g., Habeeb et al. 2015; Rennie et al. 2021), causing at least 130 deaths per year (Shiva et al. 2019). A recent study by Weinberger et al. (2020) found that excess mortality due to heat in the United States may be as much as 5000 deaths per year.

Heat stress, defined by Di Napoli et al. (2019) as "high temperatures and moisture levels . . . that can undermine the human body's ability to maintain its core temperature within the range of optimal physiological performance," represents the combined impacts of extreme heat and humidity that can be difficult for the human body to tolerate (e.g., McGregor and Vanos 2018; Raymond et al. 2020). Heat stress is particularly impactful in locations with aging populations and/or underdeveloped infrastructure; Mora et al. (2017) found that 30% of the human population is currently at risk of exposure to heat stress that exceeds a lethal threshold. That number increases to 48% and 74% under greenhouse gas emission reduction and growth scenarios, respectively. It is not just daytime heat stress that is impactful; Nissan et al. (2017) showed that anomalously warm minimum temperatures increase mortality rates, as they prohibit people from getting enough sleep. Heat stress duration is also crucial; although one day typically does not produce major impacts, three days or more pose a huge threat (e.g., Nissan et al. 2017; Di Napoli et al. 2019).

Climate change has exacerbated heat stress, often due to *combined* increases in temperature and humidity (e.g., Li et al. 2018; Di Napoli et al. 2019), resulting in larger heat-related mortality and illness rates (Willett and Sherwood 2012; Garland et al. 2015; Li et al. 2017; Raymond et al. 2017; Liao et al. 2018; Heo et al. 2019; Takakura et al. 2019), especially in urban areas (Habeeb et al. 2015; Oleson et al. 2015; Liao et al. 2018). Raymond et al. (2020) found that some places, especially subtropical coastal locations, have already exceeded the upper

Stephens's current affiliation: Department of Geological and Atmospheric Sciences, Iowa State University, Ames, Iowa.

Corresponding author: Shawn M. Milrad, milrads@erau.edu

DOI: 10.1175/JAMC-D-21-0113.1

physiological limit of wet-bulb temperature for human tolerance (35°C), although not for long durations. Overall, extreme humid heat has more than doubled in frequency in recent decades, with the annual global frequency of wet-bulb temperature exceeding 31°C shifting from fewer than 200 to greater than 400 events since 1979 (Raymond et al. 2020). However, not all regions have experienced humidity increases, and the combined increases in temperature and humidity appear most prominent in tropical and coastal subtropical locations (Raymond et al. 2020). In the United States, Grundstein and Dowd (2011) found increases (1949–2010) in apparent temperature (a metric that incorporates temperature and humidity) to be particularly prominent over the Pacific coast states and the Southeast, especially Florida. Similarly, Schoof et al. (2017) discovered increasing frequencies and spatial extents of both summer dry (temperature only) and humid (temperature and humidity) heat-wave days. However, regional caveats applied. In the southwestern United States, a desert region where subtropical drying has long been observed, these increases were driven almost entirely by warming temperatures. In other regions such as the Midwest, northern plains, and Southeast, temperature and humidity increases both played important roles in heat stress trends (Schoof et al. 2017).

Climate models project that heat stress in tropical and coastal subtropical regions will regularly exceed human tolerance levels by midcentury (Raymond et al. 2020). In the United States, extreme heat frequency, duration, and intensity are all generally projected to continue to increase, including in the Southeast (e.g., Diffenbaugh and Ashfaq 2010; Easterling et al. 2017; Herrera-Estrada and Sheffield 2017), a region dominated by a coastal subtropical climate. Smith et al. (2013) found that for 1979–2011, the Southeast had the largest land area percentage (12%) that experienced statistically significant increases in heat-wave frequency and number of heat-wave days per year. Rennie et al. (2019) also detailed statistically significant increases in Southeast extreme heat; increases in minimum temperature extremes were particularly pronounced. As Limaye et al. (2018) estimated that heat stress increases could cause 12 000 excess deaths in the eastern United States by 2050, it is vital to investigate changes in Southeast heat stress (Grundstein and Dowd 2011; Grundstein et al. 2015).

Heat stress impacts can also be enhanced by the urban heat island effect (e.g., Greene et al. 2011; Ramamurthy and Bou-Zeid 2017; Wouters et al. 2017; Ortiz and Gonzalez 2018), making urban areas with at-risk populations the most susceptible to increasing heat stress trends (e.g., Oleson et al. 2015; Rennie et al. 2021). As the U.S. population increasingly migrates southward and the Southeast becomes more urbanized, negative heat stress impacts will become more widespread.

Despite observed and projected increases in southeastern U.S. heat and humidity, heat stress studies specific to Florida are not prominent in the literature. Although its maritime climate is modified by warm-season sea breezes and the surrounding waters (especially in the Florida Peninsula), limiting the frequency of 100°F (37.8°C) temperature days (Cloutier-Bisbee et al. 2019), the combination of oppressive heat and humidity can be quite impactful. Human health and sectors such as agriculture (e.g., farm workers) are particularly affected, especially during summer. Furthermore, Florida has an increasing and older average population, as well as rapid urbanization in multiple metro areas where air conditioning is not universal (e.g., southeast Florida, Tampa Bay, Orlando). These are key risk factors for more heat-related illnesses and deaths (e.g., Florida Department of Health 2015). Keellings and Waylen (2014, 2015) found that *temperature* heat waves became more frequent, longer, and stronger in Florida during the latter half of the twentieth century. Cloutier-Bisbee et al. (2019) also found that mean, maximum, and minimum *temperature* heat waves in Florida have increased in frequency and duration at seven major Florida cities since 1950. For the same seven cities, Raghavendra et al. (2019) projected that temperature heat waves would continue to increase throughout the remainder of the twenty-first century. However, previous Florida extreme heat work did not consider the combined impacts of temperature and humidity, a gap we aim to fill.

In this study, we elucidate observations and trends in two key heat stress metrics: heat index (HI) and wet-bulb globe temperature (WBGT). Particularly during daytime, WBGT is widely considered a better estimate of heat stress impacts on the human body than HI because it incorporates wind and solar radiation, while HI only measures how hot it feels in the shade (e.g., Budd 2008; Liljegren et al. 2008; Willett and Sherwood 2012). WBGT is extremely useful for measuring heat stress during outdoor work (e.g., agriculture, construction), athletics, and military training (e.g., Liljegren et al. 2008; section 2a). However, WBGT has traditionally been a difficult metric to use in observational climate studies because of the nonstandard instrumentation and variables required to measure it. Nevertheless, established estimation formulas and recent advances in reanalysis datasets have allowed us to construct reliable hourly climatologies of WBGT since 1950 (section 2b).

Willett and Sherwood (2012) found positive WBGT trends across several large regions, although they used an older and more limited WBGT estimation method than the Liljegren et al. (2008) method used in this study. Grundstein et al. (2015) used locally "extreme" WBGTs (90th percentile) to estimate U.S. heat stress severity, finding that most of the Southeast was in their highest WBGT category. In a 4-yr study of heat stress in South Korea, Heo et al. (2019) found that WBGT more accurately diagnosed extreme heat intensity and duration than air temperature alone. Overall, WBGT has been more widely used in climate model simulations than observed climate studies. Newth and Gunasekera (2018) found that WBGT is projected to increase proportionally to greenhouse gas emissions scenario, but with increases disproportionately occurring in tropical and subtropical coastal regions, similar to the Raymond et al. (2020) results for wet-bulb temperature. Furthermore, Weatherly and Rosenbaum (2017) found that WBGT in the southern United States is projected to significantly increase by the late twenty-first century, resulting in more than 50 days per year above the U.S. military's "restricted" threshold. Meanwhile, Brouillet and Joussaume (2019) projected that future heat stress extremes in the tropics and subtropics are quite dependent on humidity extremes that may occur at different times than temperature extremes.

TABLE 1. List of the eight cities and corresponding airport ASOS stations examined in this study. ASOS stations are abbreviated using their four-letter International Civil Aviation Organization identifiers. Latitude (°N), longitude (°W), and data period used in this study are also shown. All eight locations are marked on the Fig. 1 map.

City	ASOS station	Lat (°N)	Lon (°W)	Data period used
Pensacola	KPNS	30.47	87.19	1950–2020
Tallahassee	KTLH	30.40	84.35	1950–2020
Jacksonville	KJAX	30.49	81.69	1950–2020
Daytona Beach	KDAB	29.18	81.05	1950–2020
Orlando	KMCO	28.43	81.31	1952–2020
Tampa	KTPA	27.98	82.53	1950–2020
Miami	KMIA	25.80	80.28	1950–2020
Key West	KEYW	24.55	81.76	1950–2020

Our specific objectives in this study are to

1) employ established estimation formulas to develop climatologies (1950–2020) of average summer daily maximum, mean, and minimum HI and WBGT for eight major Florida cities, using a combination of hourly surface and reanalysis data;
2) perform quantitative trend analyses of average summer daily maximum, mean, and minimum HI and WBGT at the eight Florida cities; and
3) investigate quantitative changes in exceedance frequencies for established absolute thresholds of HI and WBGT at the eight Florida cities, illuminating whether higher-end heat stress days have become more frequent over time.

2. Data, heat stress metrics, and methods

a. Data

The eight cities analyzed in this study are listed in Table 1 and marked on the map in Fig. 1. All Florida subregions are represented by at least one city, as are both coastal and inland environments. In addition, the eight cities have a wide range of population and urbanization levels. For example, Pensacola and Key West have approximate populations of 52 000 and 24 000, respectively, with relatively minimal urbanization. In contrast, the Tampa and Miami metro areas have populations of greater than 3 and 6 million, respectively, with expansive and increasing urbanization. To facilitate trend analyses, all selected stations have long hourly surface data records, starting around or before 1950 to correspond to reanalysis data availability.

Hourly surface data were taken from the NOAA National Centers for Environmental Information (NCEI) Integrated Surface Database (ISD; Smith et al. 2011). The ISD offers a reliable quality-controlled archive of hourly surface observations for 35 000 locations worldwide, including those taken from Automated Station Observing Systems (ASOS) at U.S. airports. We used the primary airport location in each city (Fig. 1; Table 1). All eight airports have data available from 1950 to present, except for Orlando (KMCO), which started in 1952 (Table 1). Our climatology period is 1950–2020, except at KMCO (1952–2020). Hourly surface temperature, dewpoint, and wind speed were downloaded to calculate our heat stress metrics.

While HI is calculated using only surface temperature and humidity (dewpoint), WBGT estimation formulas require surface wind speed and solar irradiance (section 2b). Wind speed is a standard hourly ISD variable, but solar irradiance is not. However, the recent release of the European Centre for Medium-Range Weather Forecasts (ECMWF) ERA5 reanalysis (Hersbach et al. 2020) has mitigated the solar irradiance data issue. ERA5 represents a major advance in reanalysis technology, as it has hourly global data with a horizontal resolution of 31 km. For solar irradiance, ERA5 incorporates remote sensing observations and state-of-the-art long-term forcing fields from phase 5 of the Coupled Model Intercomparison Project (CMIP5), while improving upon century-long model integrations that were originally used in the ECWMF twentieth century reanalysis (ERA-20CM; Hersbach et al. 2020). Although reanalysis solar radiation data is not a perfect substitution for observations, Hersbach et al. (2020) found that ERA5 improved substantially upon the previous ECMWF reanalysis dataset (ERA-Interim) and matched well with

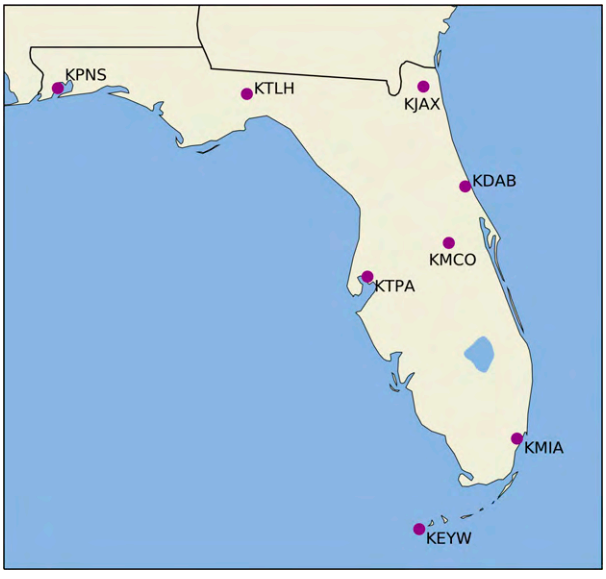

FIG. 1. Map of the eight airport locations examined in this study, marked by purple dots. The four-letter International Civil Aviation Organization airport station identifiers written in black correspond to the stations listed in Table 1.

observed irradiance data. We used the hourly surface solar radiation downward variable (Liljegren et al. 2008; Dimiceli et al. 2013) from ERA5 to estimate WBGT.

b. Heat stress metrics

1) HI

Analyzing heat stress requires choosing an appropriate metric to estimate the combined effects of temperature and humidity. In the United States, previous work has primarily used apparent temperature (AT; Steadman 1984; Grundstein and Dowd 2011) and/or HI (Rothfusz 1990). The AT variable defined by Steadman (1984) has a specific formula, while the term "apparent temperature" is sometimes used as a generic term for heat stress metrics that incorporate both temperature and humidity. Here, we focus primarily on HI, which is the primary heat stress metric used by the National Weather Service (NWS).

We use the operational NWS HI formula developed by Rothfusz (1990):

$$\mathrm{HI} = -C_0 + C_1 T + C_2 \times \mathrm{RH} - C_3 T \times \mathrm{RH} - C_4 T^2 - C_5 \times \mathrm{RH}^2 + C_6 T^2 \times \mathrm{RH} + C_7 T \times \mathrm{RH}^2 - C_8 T^2 \times \mathrm{RH}^2, \quad (1)$$

where T is surface temperature (°F), RH is surface relative humidity (%; calculated from temperature and dewpoint), and C_0–C_8 are empirically derived constants (rounded to the nearest three decimal places), as follows: $C_0 = 42.379$; $C_1 = 2.048$; $C_2 = 10.143$; $C_3 = 0.225$; $C_4 = 0.007$; $C_5 = 0.055$; $C_6 = 0.001$; $C_7 = 8.528 \times 10^{-4}$; $C_8 = 1.990 \times 10^{-6}$. For more details on the empirical constants in Eq. (1), we refer the reader to Rothfusz (1990).

Several conditional adjustments are applied to the HI calculation, again following Rothfusz (1990). HI adjustments are sometimes necessary because of parameterizations described by Rothfusz (1990); these result in the regression formula [Eq. (1)] having large errors in certain situations. When RH < 13% *and* 80° < T < 112°F (26.7°–44.4°C), Eq. (2) is used to calculate adjustment 1, which is then subtracted from the HI result in Eq. (1):

$$\text{Adjustment 1} = \frac{13 - \mathrm{RH}}{4}\frac{\sqrt{17 - |T - 95|}}{17}. \quad (2)$$

When RH > 85% *and* 80° < T < 87°F (26.7°–30.6°C), adjustment 2 is calculated using Eq. (3) and then added to the HI result from Eq. (1):

$$\text{Adjustment 2} = \left(\frac{\mathrm{RH} - 85}{10}\right)\left(\frac{87 - T}{5}\right). \quad (3)$$

When HI < 80°F (26.7°C), Eq. (4) is used instead of Eq. (1) to calculate HI:

$$\mathrm{HI} = 0.5\{T + 61.0 + [(T - 68.0)1.2] + (\mathrm{RH} \times 0.094)\}. \quad (4)$$

Once hourly HI values were calculated, we computed daily maximum, mean, and minimum values based on the methods described in section 2c.

2) WBGT

Although metrics such as the NWS HI combine heat and humidity, they struggle to diagnose heat stress impacts on human health. WBGT on the other hand, is widely considered to be a more comprehensive indicator of heat stress on the human body (Budd 2008; Lemke and Kjellstrom 2012). Originally developed by the U.S. military and used operationally by the U.S. Occupational Safety and Health Administration (OSHA), WBGT can help to manage workload and heat stress while exposed to the sun in high-temperature environments (Liljegren et al. 2008). WBGT is comprehensive primarily because it incorporates solar radiation and wind speed along with temperature and humidity.

Liljegren et al. (2008) defined the WBGT formula as

$$\mathrm{WBGT} = 0.7T_w + 0.2T_g + 0.1T_a, \quad (5)$$

where T_w (°C) is the natural wet-bulb temperature, T_g (°C) is globe temperature, and T_a (°C) is the ambient air temperature. T_a is standard in typical surface observations (e.g., ISD) but T_w and T_g are not and both require fairly complex iterative calculations (Liljegren et al. 2008).

The natural wet-bulb temperature, which accounts for 70% of WBGT, differs from the more widely used psychometric wet-bulb temperature (e.g., Stull 2011) that can be calculated from temperature and relative humidity (dewpoint). Both wet-bulb temperatures are measured using a temperature sensor with a wet wick. However, the temperature sensor in the psychometric wet-bulb measurement is typically enclosed (i.e., in the shade with an ASOS temperature sensor). In contrast, the natural wet-bulb measurement is taken with the wick entirely exposed to the outdoor environment, allowing for influences from solar radiation and wind. Because these measurements are not standard in typical surface observations, reliable estimation formulas for T_w are required. The Liljegren et al. (2008) estimation formula, used operationally by the U.S. military and OSHA, is

$$T_w = T_a - \frac{\Delta H}{c_p}\frac{M_{\mathrm{H_2O}}}{M_{\mathrm{air}}}\left(\frac{\mathrm{Pr}}{\mathrm{Sc}}\right)^a\left(\frac{e_w - e_a}{P - e_w}\right) + \frac{\Delta F_{\mathrm{net}}}{Ah}, \quad (6)$$

where T_a is the ambient air temperature, ΔH is the heat of vaporization, c_p is the specific heat at constant pressure, $M_{\mathrm{H_2O}}$ is the molecular weight of water vapor, M_{air} is the molecular weight of air, Pr is the Prandtl number, Sc is the Schmidt number, the exponent a is an empirically derived constant, e_w is the vapor pressure of the wick, e_a is the vapor pressure of the ambient air, p is pressure, ΔF_{net} is the net radiant heat flux from the environment to the wick, A is the surface area of the wick, and h is the convective heat transfer coefficient. For more details on the origin and values of the many components of the natural wet-bulb temperature [Eq. (6)] and how it is iteratively solved for, we refer the reader to Liljegren et al. (2008). Last, we highlight that at night when solar radiation is negligible, Liljegren et al. (2008) stated that the natural wet-bulb temperature can be approximated with the psychometric wet-bulb temperature (Stull 2011); we followed this procedure to calculate nighttime WBGT.

Globe temperature T_g, which accounts for 20% of WBGT [Eq. (5)], also cannot be directly measured in standard surface observations due to the lack of operational black-globe thermometers. Therefore, estimation formulas for T_g are also required, such as the Liljegren et al. (2008) method shown in Eq. (7) and used in this study:

$$T_g^4 = \frac{1}{2}(1 + \varepsilon_a)T_a^4 - \frac{h}{\varepsilon_g \sigma}(T_g - T_a) + \frac{S}{2\varepsilon_g \sigma}(1 - \alpha_g)\left\{1 + \left[\frac{1}{2\cos(\theta)} - 1\right]f_{\text{dir}} + \alpha_{\text{sfc}}\right\}, \quad (7)$$

where ε_a is atmospheric emissivity, ε_g is globe emissivity, α_g is globe albedo, α_{sfc} is surface albedo, σ is the Stefan–Boltzmann constant, T_a is ambient air temperature, h is the convective heat transfer coefficient, S is the surface solar irradiance, f_{dir} is the direct beam radiational flux defined as the ratio of the total horizontal solar irradiance to the maximum possible solar irradiance, and θ is the zenith angle. With all variables known, T_g can be iteratively solved for. For full details on the globe temperature calculation and its components, we again refer the reader to Liljegren et al. (2008).

While the Liljegren et al. (2008) estimation methods for natural wet-bulb and globe temperature have been widely used by the U.S. military and OSHA, other methods exist such as the NWS Dimiceli et al. (2013) method and one developed in Japan by Ono and Tonouchi (2014). Most estimation formulas have been reasonably accurate, at least over relatively small regions. As examples, the Liljegren et al. (2008) method exhibited an accuracy of 1°C or better at all U.S. military depots, while the Dimiceli et al. (2013) method recently became an experimental output variable in NWS forecast grids. In this study, we use the Liljegren et al. (2008) method, which has demonstrated wide applicability across several sectors (e.g., military, interscholastic athletics, agriculture). However, we caution that all WBGT estimation formulas contain some error, and work is ongoing to further improve and standardize these approximations across wide and diverse geographical regions.

Another challenge in calculating WBGT is finding reliable hourly solar radiation data. Some WBGT studies (e.g., Rennie et al. 2021) have mitigated this issue by using the U.S. Climate Reference Network (USCRN), whose stations have solar radiometers as standard instrumentation (Diamond et al. 2013). However, USCRN data only started in 2003, which is not ideal to analyze long-term WBGT trends. In this study, we used hourly ERA5 solar irradiance (section 2a) to calculate hourly WBGT values. From our hourly WBGT values, we calculated daily maximum, mean, and minimum values, as described in section 2c.

c. Methods

To build HI and WBGT climatologies, we first calculated hourly values of each metric during climatological summers [June–August (JJA)] from 1950 to 2020 [except Orlando (KMCO), where hourly data started in 1952]. Most heat stress studies use daily maximum, minimum, and/or mean values, which we calculated for both HI and WBGT from our hourly output. This strategy was used because HI and WBGT incorporate multiple atmospheric parameters, and there is no guarantee that, for example, the daily maximum WBGT will occur at the same time as the daily maximum temperature. Therefore, our daily maximum, minimum, and mean HI and WBGT are the daily maximum, minimum, and mean *hourly* values, respectively, of HI and WBGT on a given calendar day. Subsequently, average summer values of daily maximum, mean, and minimum HI and WBGT were calculated from the daily values.

At night, surface solar irradiance S is zero. Therefore, we used the Liljegren et al. (2008) method of approximating the natural wet-bulb temperature with the psychometric wet-bulb temperature (Stull 2011) when $S = 0$. In addition, by definition the entire third term in the globe temperature estimation formula [Eq. (7)] goes to zero at night when $S = 0$. As shown in section 3b, our daily minimum WBGT results are robust and align with previous studies on increasing nighttime heat stress.

Section 3 details our HI and WBGT climatologies and trend analyses. To test for statistical significance of linear trends, we used the nonparametric Mann–Kendall (MK) test through the pyMannKendall Python package (Hussain et al. 2019). The MK test is common in extreme heat studies including Cloutier-Bisbee et al. (2019). The pyMannKendall package also calculates the magnitude of linear trends using the Theil–Sen estimator (Sen's slope), which we use throughout our results in sections 3 and 4. We also used the Student's t test to evaluate statistically significant differences between the first (1950–84) and last (1986–2020) 35 years (section 3) in the HI and WBGT climatology periods. Note that all statistically significant period differences in Tables 2 and 3 are positive differences; that is, when statistically significant, the most recent 35-yr period has warmer HI and WBGT when compared with the first 35 years. Throughout our results, HI and WBGT trends (MK) and period differences (Student's t test) are considered statistically significant when p values are ≤ 0.05.

Section 4 examines exceedance frequencies for various HI and WBGT thresholds, based on NWS and OSHA standards, respectively. Figure 2a (NWS New York 2021) shows the standard NWS HI chart with threshold categories and descriptions. HI values $> 102°$ and > 124°F ($>38.9°$ and >51.1°C) are considered dangerous and extremely dangerous, respectively, with health impacts including sunstroke, muscle cramps, and/or heat exhaustion. A big difference between HI and WBGT is that WBGT values > 90°F (32.2°C) are considered extreme (Fig. 2b; Oklahoma Mesonet 2016). This can be a challenge to communicate to stakeholders and the public, who are likely more familiar with HI thresholds (Fig. 2a). We discuss these points further in sections 4 and 5.

All analyses and statistics were completed using built-in functions within MATLAB and Python's Pandas, Matplotlib, and pyMannKendall packages. The visualizations shown in Figs. 1 and 3–9 were also produced using MATLAB or Python's Matplotlib package.

TABLE 2. Statistics for the average summer (JJA) maximum, mean, and minimum daily HI observations and trends (1950–2020) shown in Figs. 3 and 4. From left to right: Linear trend (°F yr^{-1}) using the Theil–Sen estimator, Z scores and p values of the linear trends from the MK significance test, and p value from the Student's t test that evaluates positive differences (HI increases) between the first (1950–84) and last (1986–2020) 35 years in the study period. For both significance tests, results are considered to be statistically significant when $p \leq 0.05$ (marked in ***boldface italics***).

	Trend (°F yr^{-1})	Z score (MK)	p value (MK)	p value (t test)
KPNS				
Max	0.015	1.330	0.183	0.119
Mean	0.022	2.105	***0.035***	***0.018***
Min	0.026	3.683	***2.305×10^{-4}***	***8.000×10^{-4}***
KTLH				
Max	0.049	3.435	***5.929×10^{-4}***	***0.001***
Mean	0.041	4.189	***2.798×10^{-5}***	***2.646×10^{-4}***
Min	0.023	2.720	***0.007***	***0.014***
KJAX				
Max	0.018	1.281	0.200	0.089
Mean	0.010	1.072	0.284	0.082
Min	0.013	2.045	***0.041***	***0.007***
KDAB				
Max	0.062	4.099	***4.132×10^{-5}***	***3.242×10^{-6}***
Mean	0.047	4.338	***1.436×10^{-5}***	***2.005×10^{-6}***
Min	0.045	5.420	***5.950×10^{-5}***	***7.869×10^{-7}***
KMCO				
Max	0.036	3.572	***4.199×10^{-4}***	***0.002***
Mean	0.038	4.749	***2.038×10^{-6}***	***7.835×10^{-6}***
Min	0.035	5.588	***2.288×10^{-8}***	***3.517×10^{-8}***
KTPA				
Max	0.039	3.028	***0.002***	***8.000×10^{-4}***
Mean	0.060	6.234	***4.537×10^{-10}***	***1.165×10^{-8}***
Min	0.059	7.148	***8.829×10^{-13}***	***9.841×10^{-9}***
KMIA				
Max	0.064	5.261	***1.429×10^{-7}***	***2.018×10^{-9}***
Mean	0.065	6.502	***7.907×10^{-11}***	***2.902×10^{-10}***
Min	0.060	7.227	***4.936×10^{-13}***	***3.379×10^{-10}***
KEYW				
Max	0.061	5.113	***1.179×10^{-7}***	***1.059×10^{-6}***
Mean	0.054	5.381	***7.425×10^{-8}***	***1.804×10^{-6}***
Min	0.039	3.772	***1.617×10^{-4}***	***0.014***

3. Daily heat stress metrics

a. HI

Figures 3 and 4 show trends for average summer (JJA) daily maximum, mean, and minimum HI at the eight Florida cities. Accompanying linear trend values and significance test results are displayed in Table 2. For the four northern and central Florida cities shown in Fig. 3, positive trends are observed for daily maximum, mean, and minimum HI. The largest positive trends are observed at Daytona Beach (KDAB) and Tallahassee (KTLH), with the smallest at Jacksonville (KJAX). At KTLH and KDAB, all three HI parameters exhibit statistically significant positive trends and period differences (Table 2). At KDAB, much of the past half-decade features average summer daily maximum HI $\geq$ 100°F (Fig. 3d). For Pensacola (KPNS), daily mean and minimum HI increases and period differences are statistically significant, but maximum HI changes are not. Finally, at KJAX, only daily minimum HI increases are statistically significant. Similar results for KJAX were found for temperature heat waves by Cloutier-Bisbee et al. (2019), which they largely attributed to a change in station location that occurred in 1968. Prior to 1968, KJAX was located 12 km closer to downtown Jacksonville than it is now, on the banks of the Saint John's River. The post-1968 (and current) airport location, however, is in a rural forested area well northwest of downtown, and the linear trend since approximately the late 1970s is positive while the trend before that time is negative (Fig. 3c). Many studies (e.g., Ramamurthy and Bou-Zeid 2017; Wouters et al. 2017; Ortiz and Gonzalez 2018) have found that urban heat islands can have notable impacts on extreme heat, and the move of KJAX to a more rural inland location during the study period likely resulted in considerably smaller overall positive trends. KJAX is the only station that experienced a location change during our climatology period.

All four central and southern Florida cities shown in Fig. 4 exhibit statistically significant positive trends and period differences in average summer daily maximum, mean, and minimum HI (Table 2). The largest trends in each HI variable among all eight stations are observed at Miami (KMIA). Tampa (KTPA) also exhibits large increases in daily mean

TABLE 3. As in Table 2, but for the average summer daily WBGT observations and trends (1950–2020) displayed in Figs. 5 and 6.

	Trend (°F yr^{-1})	Z score (MK)	p value (MK)	p value (t test)
KPNS				
Max	0.003	0.288	0.773	0.184
Mean	0.015	2.690	***0.007***	***0.001***
Min	0.032	2.432	***0.015***	0.184
KTLH				
Max	0.012	1.744	0.081	***0.065***
Mean	0.040	5.083	$\boldsymbol{3.720 \times 10^{-7}}$	$\boldsymbol{5.960 \times 10^{-6}}$
Min	0.049	0.318	$\boldsymbol{9.180 \times 10^{-5}}$	***0.001***
KJAX				
Max	0.014	2.035	***0.042***	0.065
Mean	0.030	5.489	$\boldsymbol{4.030 \times 10^{-8}}$	$\boldsymbol{2.000 \times 10^{-4}}$
Min	0.044	3.157	***0.002***	$\boldsymbol{2.000 \times 10^{-4}}$
KDAB				
Max	0.033	4.001	$\boldsymbol{6.320 \times 10^{-5}}$	$\boldsymbol{1.150 \times 10^{-5}}$
Mean	0.047	7.078	$\boldsymbol{1.460 \times 10^{-12}}$	$\boldsymbol{1.540 \times 10^{-12}}$
Min	0.069	5.311	$\boldsymbol{1.090 \times 10^{-7}}$	$\boldsymbol{1.170 \times 10^{-5}}$
KMCO				
Max	−0.014	−1.870	0.062	***0.038***
Mean	0.015	3.299	***0.001***	***0.018***
Min	0.041	4.646	$\boldsymbol{3.380 \times 10^{-6}}$	$\boldsymbol{8.980 \times 10^{-5}}$
KTPA				
Max	0.024	2.948	***0.003***	$\boldsymbol{2.000 \times 10^{-4}}$
Mean	0.038	6.820	$\boldsymbol{9.100 \times 10^{-12}}$	$\boldsymbol{3.460 \times 10^{-13}}$
Min	0.049	5.400	$\boldsymbol{6.650 \times 10^{-8}}$	$\boldsymbol{9.020 \times 10^{-6}}$
KMIA				
Max	0.023	2.859	***0.004***	$\boldsymbol{2.000 \times 10^{-4}}$
Mean	0.037	7.058	$\boldsymbol{1.690 \times 10^{-12}}$	$\boldsymbol{2.050 \times 10^{-11}}$
Min	0.033	5.281	$\boldsymbol{1.280 \times 10^{-7}}$	$\boldsymbol{2.000 \times 10^{-4}}$
KEYW				
Max	0.010	1.747	0.081	***0.018***
Mean	0.023	4.864	$\boldsymbol{1.150 \times 10^{-6}}$	$\boldsymbol{9.900 \times 10^{-6}}$
Min	0.024	2.700	***0.007***	***0.005***

and minimum HI, while Key West (KEYW) does the same for daily maximum and mean HI. Interestingly, recent summers at KEYW (Fig. 4d) feature average summer daily maximum HI values > 100°F and daily minimum HI values in the upper 80°Fs; both are the hottest of any city in our study and represent a dangerous recent escalation in heat stress conditions.

All eight cities, even Jacksonville despite the station relocation, exhibit statistically significant increases and period differences in daily minimum HI (Table 3). These results are consistent with the Fourth U.S. National Climate Assessment (Carter et al. 2018) as well as other recent studies (e.g., Mora et al. 2017; Nissan et al. 2017; Rennie et al. 2019) that have found daily minimum temperatures are increasing as quickly or even faster than daily maximum temperatures in many places, including the Southeast (Carter et al. 2018). While our daily minimum HI positive trends are only larger than daily maximum HI trends at two stations (KPNS and KTPA; Table 2), only six of eight daily maximum HI increases are statistically significant while all eight daily minimum HI increases are significant.

It is likely not coincidental that the largest summer HI increases (Table 2) occur at KDAB (0.062°, 0.047°, and 0.045°F yr^{-1} (1 Celsius degree = 5/9ths of a Fahrenheit degree) for daily maximum, mean, and minimum, respectively), KTPA (0.039°, 0.060°, and 0.059°F yr^{-1}, respectively), KMIA (0.064,° 0.065°, and 0.060°F yr^{-1}, respectively), and KEYW (0.061°, 0.054°, and 0.039°F yr^{-1}, respectively). These four locations are located closest to large warm bodies of water (Atlantic Ocean; Gulf of Mexico). Several studies for the eastern United States and Caribbean (e.g., Little et al. 2015; Taylor and Clarke 2018) have causally linked extreme heat increases at subtropical coastal locations to warmer sea surface temperatures (SSTs), while Raymond et al. (2020) found coastal subtropical locations exhibit the most dangerous heat stress values on Earth. Warmer SSTs promote more evaporation that increases atmospheric water vapor (dewpoint), which in turn can increase HI and WBGT.

Overall, Florida Peninsula locations exhibit larger positive HI trends than Panhandle locations (Figs. 3 and 4; Table 2), except for daily maximum and mean HI at Orlando (KMCO) relative to KTLH. Some of these differences can likely be attributed to the proximity of water, as four (KDAB, KTPA, KMIA, KEYW) of the five Peninsula stations are coastal locations. However, we also note that parts of the Southeast (particularly north of the Florida Peninsula) were relatively slow to warm, and at times cooled, during the latter half of the twentieth century (e.g., Meehl et al. 2012). This has long been dubbed the "southeast warming hole," caused by a

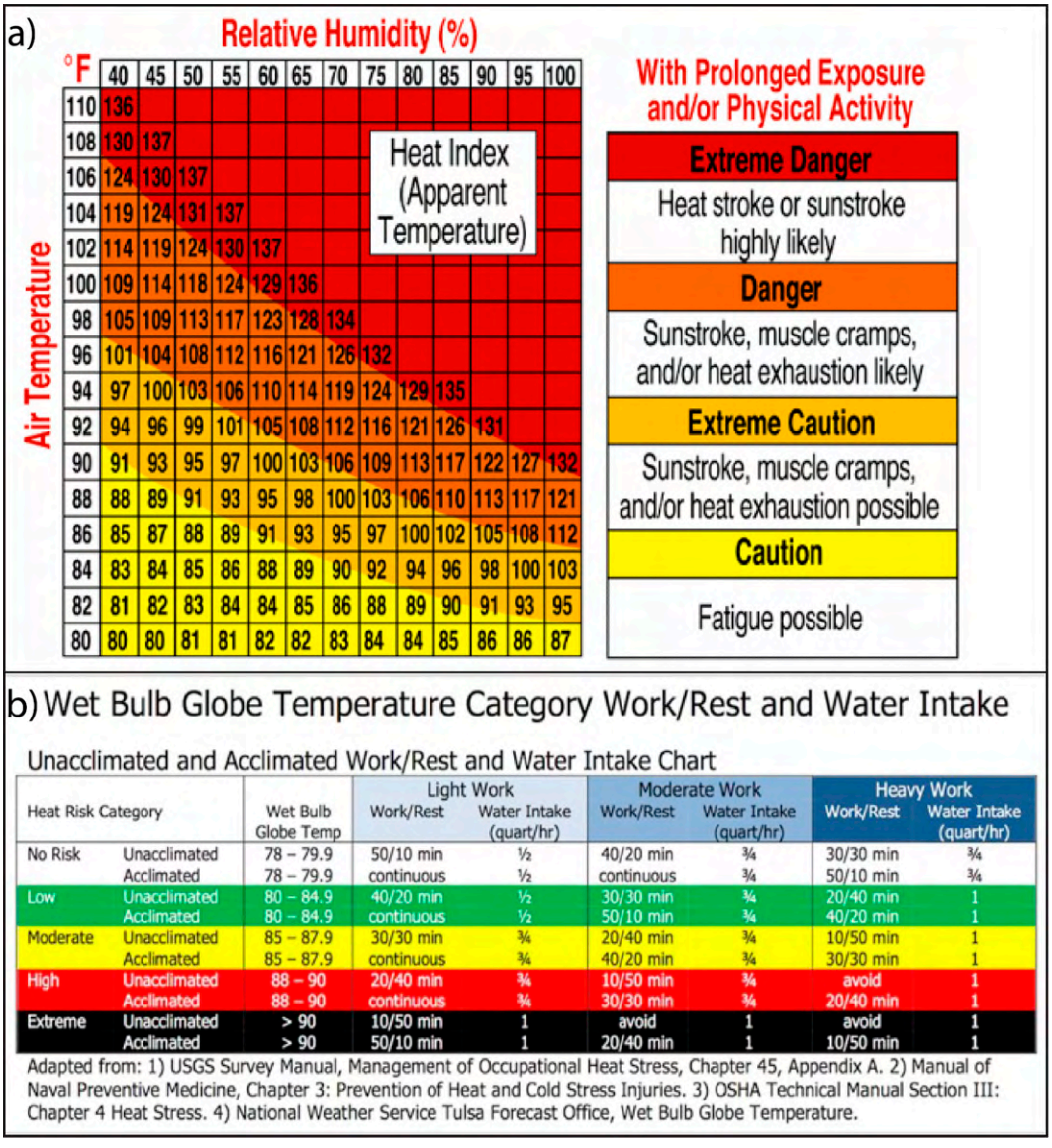

Heat Risk Category		Wet Bulb Globe Temp	Light Work Work/Rest	Light Work Water Intake (quart/hr)	Moderate Work Work/Rest	Moderate Work Water Intake (quart/hr)	Heavy Work Work/Rest	Heavy Work Water Intake (quart/hr)
No Risk	Unacclimated	78 – 79.9	50/10 min	½	40/20 min	¾	30/30 min	¾
	Acclimated	78 – 79.9	continuous	½	continuous	¾	50/10 min	¾
Low	Unacclimated	80 – 84.9	40/20 min	½	30/30 min	¾	20/40 min	1
	Acclimated	80 – 84.9	continuous	½	50/10 min	¾	40/20 min	1
Moderate	Unacclimated	85 – 87.9	30/30 min	¾	20/40 min	¾	10/50 min	1
	Acclimated	85 – 87.9	continuous	¾	40/20 min	¾	30/30 min	1
High	Unacclimated	88 – 90	20/40 min	¾	10/50 min	¾	avoid	1
	Acclimated	88 – 90	continuous	¾	30/30 min	¾	20/40 min	1
Extreme	Unacclimated	> 90	10/50 min	1	avoid	1	avoid	1
	Acclimated	> 90	50/10 min	1	20/40 min	1	10/50 min	1

Adapted from: 1) USGS Survey Manual, Management of Occupational Heat Stress, Chapter 45, Appendix A. 2) Manual of Naval Preventive Medicine, Chapter 3: Prevention of Heat and Cold Stress Injuries. 3) OSHA Technical Manual Section III: Chapter 4 Heat Stress. 4) National Weather Service Tulsa Forecast Office, Wet Bulb Globe Temperature.

FIG. 2. Operational threshold categories and corresponding impacts of (a) heat index as defined by the NWS (NWS New York 2021) and (b) wet bulb globe temperature as defined by OSHA (Oklahoma Mesonet 2016). The HI categories analyzed in this study and shown in (a) are 80°–90°F (caution), 91°–102°F (extreme caution), 103°–124°F (danger), and ≥125°F (51.7°C) (extreme danger). The WBGT categories shown in (b) that are used in this study are 85–87.9°F (moderate), 88°–90°F (high), and >90°F (extreme).

multitude of factors including natural variability, increased cloud cover, and land surface processes (Meehl et al. 2012; Rogers 2013; Partridge et al. 2018). Yet even during the "warming hole" era, heat waves in the southeast United States still increased in frequency, duration, and intensity (Smith et al. 2013). Furthermore, the southeast United States has experienced a distinct warming trend since the start of the twenty-first century (Meehl et al. 2012; Smith et al. 2013). Based on Figs. 3 and 4, as well as the statistically significant changes shown in Table 2, our results largely align with the idea that while the Southeast warming hole was notable during the mid–late-twentieth century, warming has accelerated over the past three or four decades.

Of our eight stations, KMCO, KTPA, and KMIA experienced the largest urbanization over the past few decades (Keellings and Waylen 2014; Cloutier-Bisbee et al. 2019), as the Orlando, Tampa Bay, and Miami metro areas have expanded rapidly. However, as Cloutier-Bisbee et al. (2019) found for temperature heat waves, summer HI trends at KDAB and KEYW are comparable to those at KTPA and KMIA, and larger than those at KMCO. Direct comparisons (Figs. 3 and 4; Table 2) between KMIA and KEYW

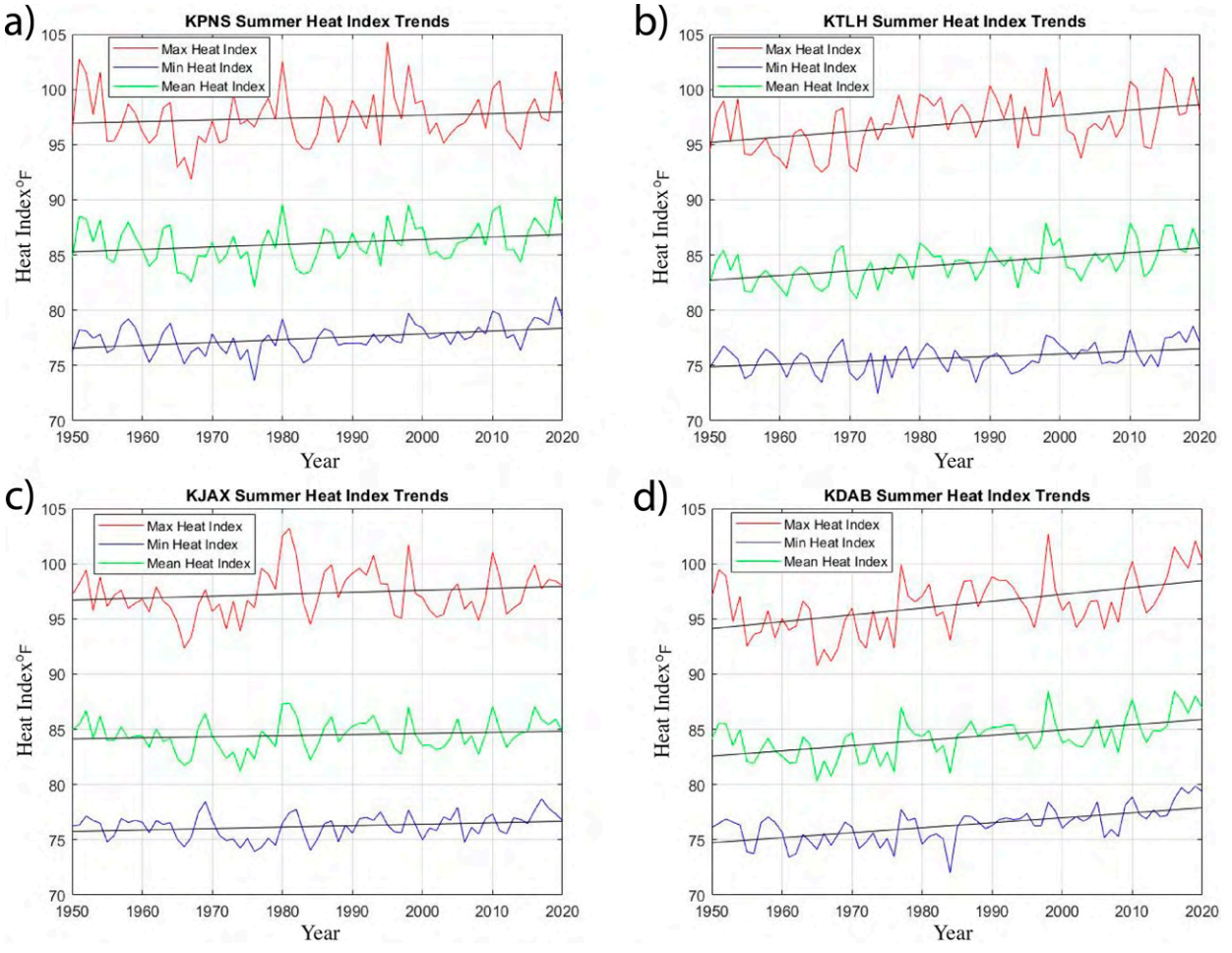

FIG. 3. Observations and linear trends in average summer (JJA) daily maximum (red), mean (green), and minimum (blue) HI (1950–2020) for (a) KPNS, (b) KTLH, (c) KJAX, and (d) KDAB, the four northernmost stations in this study. Linear trend lines (solid black) for each variable are based on the Theil–Sen estimator, with the corresponding values (°F yr^{-1}) displayed in Table 2. The Z scores and p values of trends based on the MK significance test, as well as p values from the Student's t test evaluating differences between the first (1950–84) and last (1986–2020) 35 years in the study period, are also shown in Table 2. Trends (MK) and period differences (Student's t test) are deemed statistically significant when $p \leq 0.05$.

(approximately 255 km apart) as well as between KDAB and KMCO (approximately 110 km apart) suggest that urbanization plays a minimal role in summer HI trends. Both Daytona Beach and Key West have urbanized much more slowly than Orlando, Tampa Bay, and Miami, while Key West's current population is roughly the same as it was in 1950.

b. WBGT

Figures 5 and 6 show trends in average summer daily maximum, mean, and minimum WBGT at the eight Florida cities. Corresponding trend values and significance test results are displayed in Table 3.

For the four northernmost cities (Fig. 5), statistically significant increases and period differences are observed across the board in summer daily minimum and mean WBGT, except for daily minimum WBGT period differences at KPNS (Table 3). Daily maximum WBGT increases at all four cities, but the linear trends are only statistically significant at KDAB and KJAX, while period differences are statistically significant only at KDAB and KTLH (Table 3). The largest positive trends for each WBGT variable are observed at KDAB (0.033°, 0.047°, and 0.069°F yr^{-1} for daily maximum, mean, and minimum WBGT, respectively). Interestingly, daily minimum WBGT increases outpace daily maximum and mean values at all four cities (Table 3), supporting the assertion of faster warming nights in the region (e.g., Carter et al. 2018). Despite the station location change, the trends in all three WBGT metrics are significantly positive at KJAX.

Results for the four southernmost cities (Fig. 6; Table 3) show that like the four northern cities, average summer daily maximum, mean, and minimum WBGT increase across with the board, with the single exception of a small insignificant decrease in daily maximum WBGT at KMCO. Increases and period differences in daily mean and minimum WBGT are statistically significant at all four southernmost cities, and at KMCO both daily mean and minimum WGBT increase

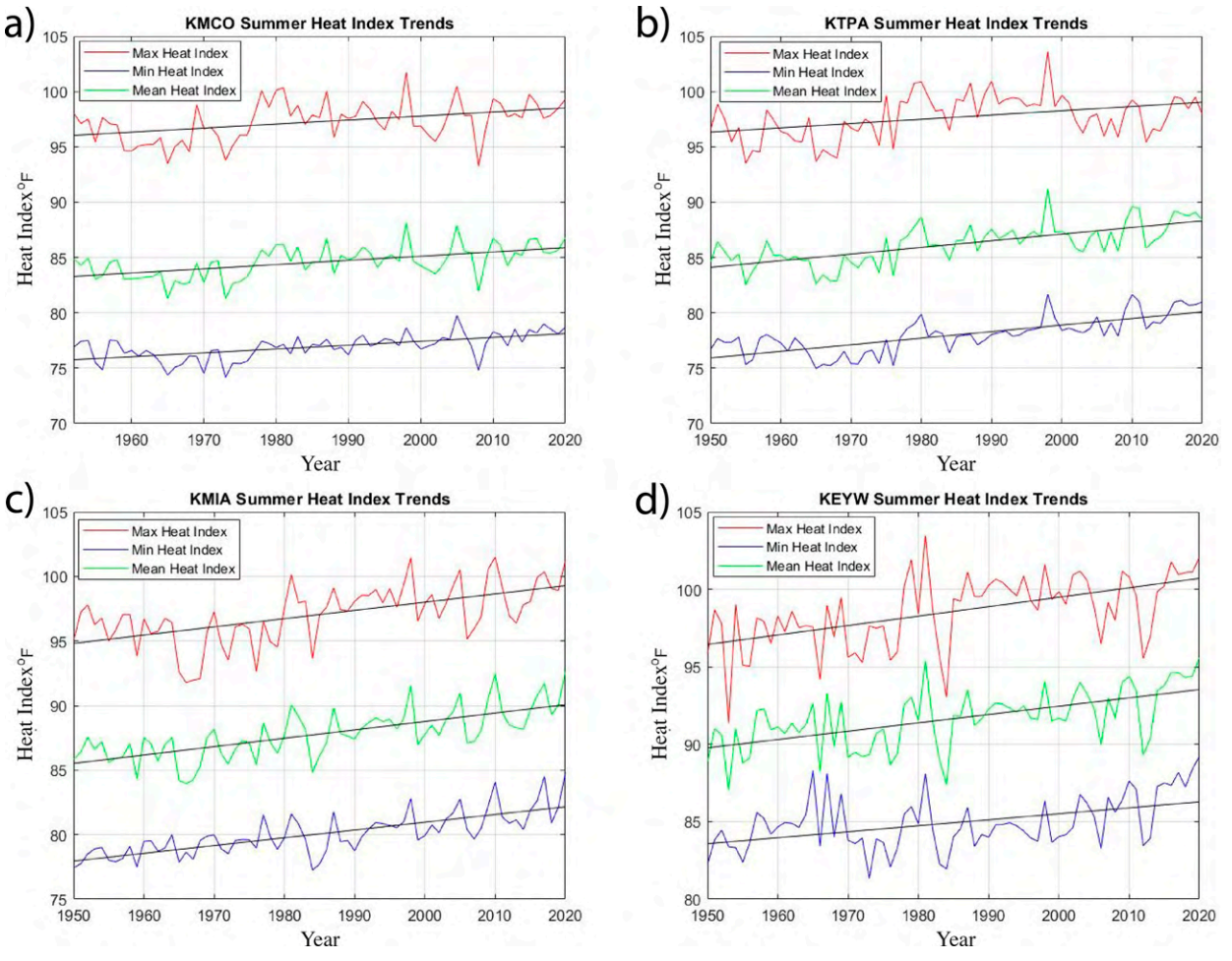

FIG. 4. As in Fig. 3, but for (a) KMCO, (b) KTPA, (c) KMIA, and (d) KEYW, the four southernmost stations in this study. Corresponding statistics and significance test results are shown in Table 2. Note that all stations except KMCO start in 1950; KMCO data start in 1952 (Table 1).

significantly (Table 3). The largest increases among the southernmost cities occur at KTPA (0.024°, 0.038°, and 0.049°F yr^{-1}, respectively), with KMIA (0.023°, 0.037°, and 0.033°F yr^{-1}, respectively) a close second. Interestingly, increases at KTPA and KMIA are still smaller than the increases at KDAB (0.033°, 0.047°, and 0.069°F yr^{-1}, respectively). This differs slightly from our HI results, in which the increases at KTPA and KMIA largely outpaced KDAB.

A key takeaway from our WBGT trend analysis is that daily mean and minimum WBGT exhibit significant increases at all eight stations, while daily maximum WBGT does so at five of eight locations (excluding KPNS, KTLH, and KMCO). Another important result is that, of the eight locations that we examined, KDAB, KTPA, and KMIA have the largest (and entirely statistically significant) increases in daily maximum, mean, and minimum HI and WBGT. This further supports our hypothesis that urbanization is not a primary factor in Florida heat stress increases, as Daytona Beach has seen much less urbanization and population growth than Tampa and Miami over the past several decades. However, it suggests that warming SSTs at coastal subtropical locations such as Daytona Beach, Tampa, and Miami are important, as reported by other studies (e.g., Little et al. 2015; Raymond et al. 2020).

In particular during the past decade, all eight cities exhibit *average* summer daily maximum WBGTs of 88°–91°F (31.1°–32.8°C) (Figs. 5 and 6), considered to be "high" to "extreme" by OSHA (Fig. 2b). These very warm WBGT values have a profound impact on human health and industry workers (e.g., agriculture) throughout the state, and our results emphasize that summer WBGTs are only increasing with time. To further understand these changes, section 4 quantifies trends in HI and WBGT threshold value exceedance frequencies.

4. Threshold exceedance frequencies

a. HI

In this section, we investigate trends in exceedance frequencies for the absolute NWS HI thresholds defined in Fig. 2a. The histograms in Figs. 7 and 8 show the number of summer

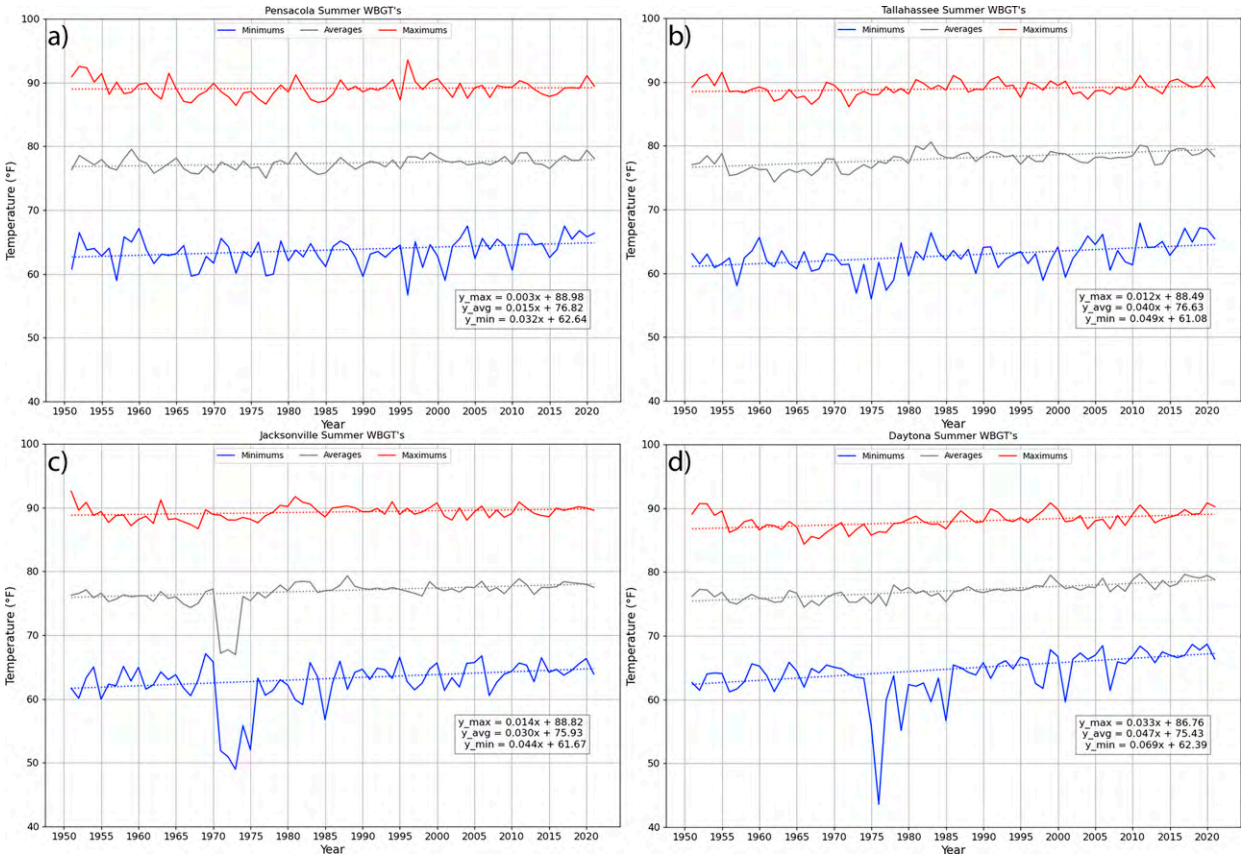

FIG. 5. Observations and linear trends in average summer (JJA) daily maximum (red), mean (gray), and minimum (blue) WBGT (1950–2020) at (a) KPNS, (b) KTLH, (c) KJAX, and (d) KDAB. Linear trend lines (dashed) for each variable are based on the Theil–Sen estimator, with the corresponding values (°F yr^{-1}) displayed in Table 3. The Z scores and p values of trends based on the MK significance test, as well as p values from the Student's t test evaluating differences between the first (1950–84) and last (1986–2020) 35 years in the study period, are also shown in Table 3. Trends (MK) and period differences (Student's t test) are deemed statistically significant when $p \leq 0.05$.

days per year in which the NWS thresholds are exceeded for daily maximum and minimum HI, respectively. Corresponding trend values and significance test results for daily maximum HI are shown in Table 4. While the NWS thresholds specified in Fig. 2a are largely designed for daily maximum HI to communicate daytime heat stress impacts (NWS New York 2021), we find it useful to also apply them to daily minimum HI, given threat to human health posed by increasing nighttime heat stress (e.g., Nissan et al. 2017; Carter et al. 2018).

Six of the eight cities (excluding KPNS and KJAX) exhibit statistically significant increases in the frequency of danger (103°–124°F) (39.4°–51.1°C) daily maximum HI days since 1950 (Table 4; Fig. 7). Perhaps unsurprisingly, at all six stations where danger days significantly increase, the frequency of caution (80°–90°F) (26.7°–32.2°C) days significantly decreases (Table 4). Extreme caution (91°–102°F) (32.8°–38.9°C) days also decrease at the six stations but only KMIA exhibits a significant decrease (Table 4). At KPNS and KJAX, both danger and extreme caution days increase in frequency at the expense of caution days, but these changes are not statistically significant (Table 4). Nevertheless, our results show that there is a substantial increase in the ratio of danger to caution days since 1950, indicating that higher-end heat stress days (based on HI) have become more frequent across Florida, particularly in the Peninsula. The largest increases in danger HI days are observed at KEYW (0.339 days yr^{-1}), KMIA (0.221 days yr^{-1}), and KDAB (0.214 days yr^{-1}), coastal subtropical locations (Raymond et al. 2020) located adjacent to warming large bodies of water (e.g., Little et al. 2015). These finding are exemplified by Daytona Beach experiencing > 30 danger HI days per summer in four of the most recent five years in our study (2016–20; Fig. 7d), while Key West had > 20 danger days during each of the final seven years in our climatology (2014–20; Fig. 7h).

While the NWS absolute HI thresholds are designed for daily maximum HI, Fig. 8 shows histograms of those thresholds for daily minimum HI. Because only one threshold category is represented at five stations and two categories at three stations (Fig. 8), we do not include a table of trend statistics. Nevertheless, Fig. 8 shows threshold exceedance frequency increases that correspond to the statistically significant daily

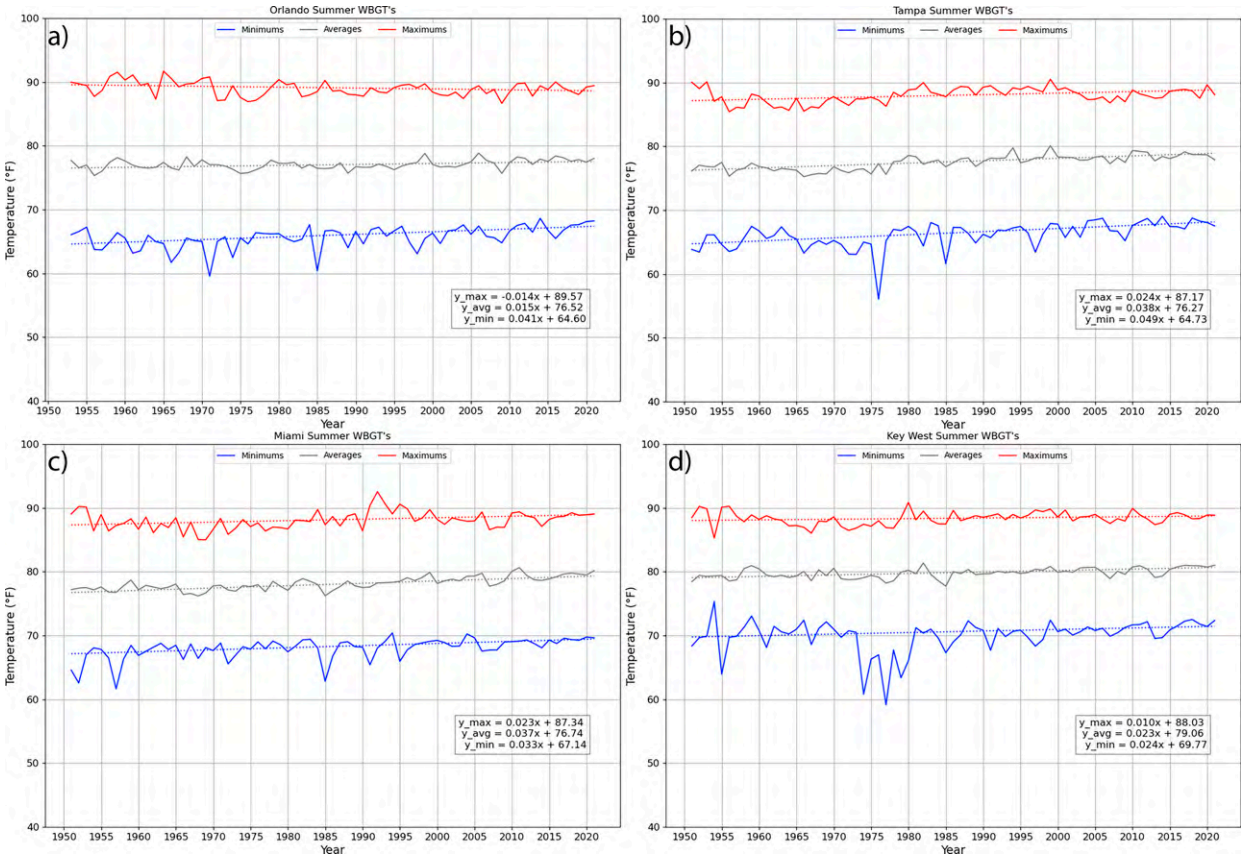

FIG. 6. As in Fig. 5, but for (a) KMCO, (b) KTPA, (c) KMIA, and (d) KEYW. Corresponding statistics and significance test results are shown in Table 3. Note that all stations except KMCO start in 1950; KMCO data start in 1952 (Table 1).

minimum HI trends shown in Figs. 2 and 3. At the three cities (Miami, Tampa, and Daytona Beach) with the largest daily minimum HI increases (Table 2), the frequency of caution or extreme caution daily minimum HI days exhibit statistically significant increases (Fig. 8; statistics not shown). At KDAB, only two years (1998 and 2010) prior to 2016 have > 20 caution daily minimum HI days, while every year during 2016–20 has >20, three of which have >30 days (Fig. 8d). Similar trends for a larger raw number of days are observed at KTPA (Fig. 8f) and KMIA (Fig. 8g). At KEYW, the number of caution daily minimum HI days actually decreases in recent years because the number of extreme caution days increases. This suggests that the escalation in Florida summer heat stress is not limited to daytime, and that nighttime conditions pose an increasing threat to human health, especially in coastal locations and south Florida.

b. WBGT

Figure 9 shows the number of summer days in each year in which three daily maximum WBGT absolute thresholds (moderate, high, extreme; Fig. 2b) are exceeded. Corresponding trend values and significance test results for daily maximum WBGT are shown in Table 5. Only results for daily maximum WBGT are shown because the thresholds outlined by OSHA (Fig. 2b) are defined in part based on exposure to solar radiation (Oklahoma Mesonet 2016). OSHA defines extreme WBGT as >90°F, for which they recommend avoiding most outdoor work, especially if unacclimated (Fig. 2b). These WBGT thresholds can pose perception and communication issues with the public and end users, who are likely more used to HI values, and do not consider a value of 90°F to be "extreme" (Rennie et al. 2021).

There are statistically significant increases in the frequency of moderate and high WBGT summer days at seven (excluding KTLH) and six (excluding KPNS and KMCO) of eight locations, respectively (Fig. 9; Table 5). The largest statistically significant positive trends in high WBGT days occur at KEYW (0.120 days yr^{-1}), KDAB (0.091 days yr^{-1}), and KMIA (0.081 days yr^{-1}), corresponding to the larger positive trends in daily maximum WBGT (Figs. 5 and 6; Table 3). Overall, it is evident that the frequency of hazardous heat stress as defined by WBGT is largely increasing throughout the state, particularly in coastal central and southern Florida, similar to our HI results (section 4a).

The results shown in Fig. 8 also highlight a limitation to using absolute thresholds for heat stress metrics. While OSHA defines WBGT > 90°F as "extreme" (Oklahoma Mesonet 2016), not many days in our climatology meet this

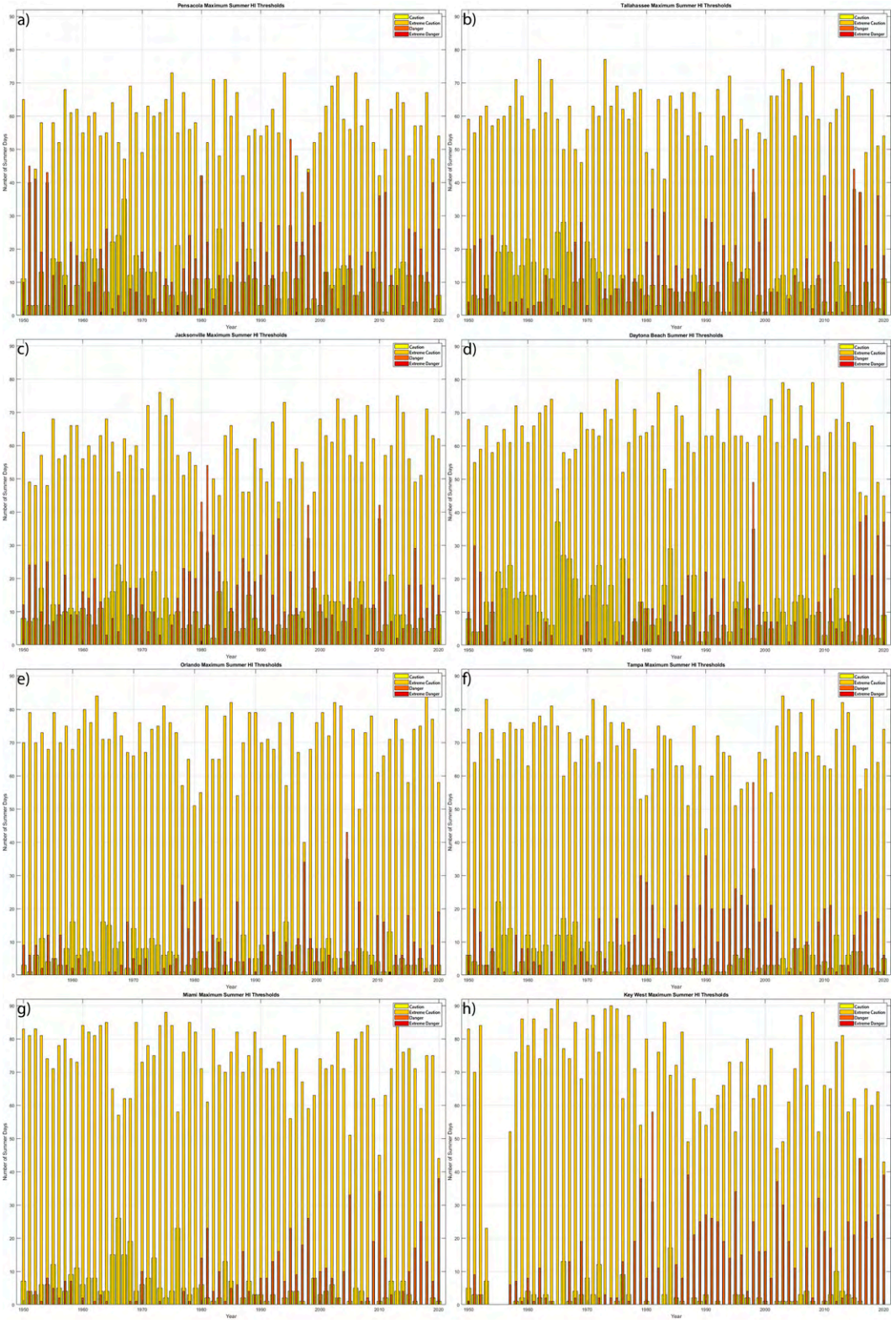

FIG. 7. Frequency histograms (days yr^{-1}) of summer (JJA) daily maximum HI that fit the caution (yellow), extreme caution (pale orange), danger (orange), and extreme danger (red) threshold categories defined in Fig. 2a. Corresponding statistics are shown in Table 4. Shown here are (a) KPNS, (b) KTLH, (c) KJAX, (d) KDAB, (e) KMCO, (f) KTPA, (g) KMIA, and (h) KEYW. All histograms are for 1950–2020, except for KMCO (1952–2020).

FIG. 8. As in Fig. 7, but for summer daily minimum HI.

TABLE 4. Statistics for the average summer daily maximum HI threshold category trends shown in Fig. 7. From left to right: threshold category (Fig. 2a) and number n of events in each category throughout the climatology period, linear trends (summer days yr^{-1}) using the Theil–Sen estimator, and Z scores and p values of the linear trends from the MK significance test. Results are considered to be statistically significant when $p \leq 0.05$ (marked in ***boldface italics***). "NA" indicates categories with five or fewer days in our study period.

Category	Trend (days yr^{-1})	Z score (MK)	p value (MK)
KPNS			
Caution (n = 766)	−0.066	−1.547	0.122
Extreme caution (n = 4041)	0.007	0.104	0.916
Danger (n = 1264)	0.051	1.039	0.299
Extreme danger (n = 5)	NA	NA	NA
KTLH			
Caution (n = 725)	−0.135	−3.727	***1.940 × 10^{-4}***
Extreme caution (n = 4230)	−0.064	−0.651	0.515
Danger (n = 980)	0.184	0.057	***0.006***
Extreme danger (n = 0)	NA	NA	NA
KJAX			
Caution (n = 712)	−0.037	−1.390	0.163
Extreme caution (n = 4111)	0.031	0.701	0.483
Danger (n = 1128)	0.029	0.069	0.945
Extreme danger (n = 1)	NA	NA	NA
KDAB			
Caution (n = 803)	−0.146	−3.211	***0.001***
Extreme caution (n = 4534)	−0.034	−0.164	0.869
Danger (n = 722)	0.214	3.457	***5.463 × 10^{-4}***
Extreme danger (n = 0)	NA	NA	NA
KMCO			
Caution (n = 419)	−0.049	−2.021	***0.043***
Extreme caution (n = 4866)	−0.069	−0.539	0.589
Danger (n = 592)	0.105	2.139	***0.032***
Extreme danger (n = 2)	NA	NA	NA
KTPA			
Caution (n = 393)	−0.068	−1.850	***0.064***
Extreme caution (n = 4874)	−0.077	−1.467	0.142
Danger (n = 847)	0.125	2.049	***0.040***
Extreme danger (n = 0)	NA	NA	NA
KMIA			
Caution (n = 374)	−0.115	−4.687	***2.769 × 10^{-6}***
Extreme caution (n = 5216)	−0.161	−2.606	***0.009***
Danger (n = 546)	0.221	4.376	***1.209 × 10^{-5}***
Extreme danger (n = 0)	NA	NA	NA
KEYW			
Caution (n = 169)	−0.025	−1.310	0.189
Extreme caution (n = 4737)	−0.009	−2.430	0.151
Danger (n = 966)	0.339	4.970	***6.490 × 10^{-7}***
Extreme danger (n = 0)	NA	NA	NA

threshold, at least based on the Liljegren et al. (2008) estimation formula. This is likely in part due to temperatures in Florida rarely exceeding 100°F, as a function of the warm-season sea breezes and maritime climate (e.g., Cloutier-Bisbee et al. 2019). In the next section, we propose additional analysis techniques and threshold definitions to improve the robustness of WBGT trend investigations regardless of region.

5. Discussion and conclusions

This study develops climatologies and trend analyses (1950–2020) of two heat stress metrics (HI and WBGT) at eight representative cities across Florida. HI and WBGT are calculated with established formulas used operationally by NWS (Rothfusz 1990) and OSHA (Liljegren et al. 2008), respectively. Hourly solar radiation data from the ERA5 reanalysis (Hersbach et al. 2020) are used to calculate hourly WBGT, something that was not previously possible at most existing surface (ASOS) stations.

Our analysis shows that average summer daily maximum, mean, and minimum summer HI increase significantly at all eight cities, except for daily maximum HI at Pensacola and daily maximum and mean HI at Jacksonville (Figs. 3 and 4; Table 2). With the aforementioned few exceptions, the most

FIG. 9. Frequency histograms (days yr^{-1}) of summer (JJA) daily maximum WBGT that fit the moderate (yellow), high (red), and extreme (black) threshold categories defined in Fig. 2b. Corresponding statistics are shown in Table 5. Shown here are (a) KPNS, (b) KTLH, (c) KJAX, (d) KDAB, (e) KMCO, (f) KTPA, (g) KMIA, and (h) KEYW. All histograms are for 1950–2020, except for KMCO (1952–2020).

TABLE 5. Statistics for the average summer daily maximum WBGT threshold category trends shown in Fig. 9. From left to right: threshold category (Fig. 2b) and number n of events in each category throughout the climatology period, linear trends (days yr^{-1}) using the Theil–Sen estimator, and Z scores and p values of the linear trends from the MK significance test. Results are considered to be statistically significant when $p \leq 0.05$ (marked in ***bold italics***).

Category	Trend (days yr^{-1})	Z score (MK)	p value (MK)
KPNS			
Moderate (n = 2427)	0.136	−0.423	***0.006***
High (n = 535)	0	0.622	0.534
Extreme (n = 145)	0	1.356	0.175
KTLH			
Moderate (n = 2600)	0.111	1.869	0.062
High (n = 623)	0.098	2.910	***0.004***
Extreme (n = 122)	0	0.247	0.805
KJAX			
Moderate (n = 2606)	0.212	4.722	$\boldsymbol{2.339 \times 10^{-6}}$
High (n = 681)	0.071	2.119	***0.034***
Extreme (n = 141)	0	0.445	0.656
KDAB			
Moderate (n = 2306)	0.458	5.423	$\boldsymbol{5.861 \times 10^{-8}}$
High (n = 337)	0.091	3.857	$\boldsymbol{1.148 \times 10^{-4}}$
Extreme (n = 51)	0	0.496	0.620
KMCO			
Moderate (n = 2950)	0.226	3.909	$\boldsymbol{9.269 \times 10^{-5}}$
High (n = 565)	0	0.362	0.718
Extreme (n = 80)	−0.020	−3.138	***0.002***
KTPA			
Moderate (n = 2979)	0.363	4.551	$\boldsymbol{5.328 \times 10^{-6}}$
High (n = 338)	0.042	1.635	0.102
Extreme (n = 21)	0	0	1
KMIA			
Moderate (n = 2762)	0.519	5.737	$\boldsymbol{9.649 \times 10^{-9}}$
High (n = 244)	0.081	4.035	$\boldsymbol{5.456 \times 10^{-5}}$
Extreme (n = 28)	0	−0.484	0.628
KEYW			
Moderate (n = 3835)	0.306	4.680	$\boldsymbol{2.863 \times 10^{-6}}$
High (n = 461)	0.120	3.495	$\boldsymbol{4.734 \times 10^{-4}}$
Extreme (n = 23)	0	−1.502	0.133

recent 35-yr period in our climatology (1986–2020) also exhibits significantly higher HI than the first 35-yr period (1950–84). Jacksonville is unique in that the airport location (KJAX) moved to a more rural and inland location during our climatology period (section 3a). The largest HI increases occur at Daytona Beach, Tampa, Miami, and Key West, all of which are coastal subtropical locations more prone to heat stress increases due to warming SSTs and increased evaporation (Raymond et al. 2020). Daily mean and minimum WBGT exhibit statistically significant increases at all eight Florida cities, while daily maximum WBGT increases significantly at five of eight locations (Figs. 4 and 5; Table 3). Positive trends are largest at Daytona Beach, Miami, and Tampa (Table 3), similar to our HI results.

Across-the-board significant increases in daily minimum HI (Table 2) and WBGT (Table 3) are also consistent with recent studies (e.g., Mora et al. 2017; Nissan et al. 2017; Rennie et al. 2019), emphasizing how much nighttime heat stress can negatively impact human health. This is also highlighted by the increase in caution and extreme caution daily minimum HI events (Fig. 8), despite the threshold categories being defined for daily maximum HI. Urbanization, however, does not appear to play a large role in Florida heat stress increases; despite very different populations and urbanization levels, Daytona Beach exhibits larger positive HI and WGBT trends than nearby Orlando, while Key West and nearby Miami are similar (Tables 2 and 3).

In terms of NWS HI thresholds (Fig. 2a), the frequency of danger (103°–124°F) summer HI days increases significantly at most locations across Florida (Fig. 7; Table 4). The increased prevalence of danger days comes at the expense of caution (80°–90°F) days, emphasizing a substantial intensification of heat stress across the state. The largest increases in extreme caution days are found at Key West, Miami, and Daytona Beach, largely mirroring the increases in daily maximum HI. However, there are still very few Florida summer days classified in the "extreme danger" (>124°F) category. This emphasizes the limitations of using national absolute thresholds for heat stress and suggests that relative (i.e., percentile-based) and/or regional thresholds may be a better approach (Rennie et al. 2021).

For WBGT thresholds (Fig. 2b), statistically significant increases in the frequency of high (88°–90°F) days occur at five cities, while similar results for moderate (85°–87.9°F) (29.4°–31.05°C) days are observed in seven cities (Table 5; Fig. 9). However, few days in our climatology meet the "extreme" (>90°F) WBGT category, likely due to the lack of 100°F temperatures in Florida's maritime climate. Again, this emphasizes the limitations of national absolute thresholds for heat stress metrics.

Overall, HI and WBGT trends both elucidate a substantial escalation in summer heat stress across the state, particularly at coastal locations in the Florida Peninsula and Keys. While acclimation to extreme WBGT conditions can help (Fig. 2a), widespread increases in heat stress have substantial impacts on human health, especially for occupations (e.g., agricultural workers) that necessitate being outdoors for long durations.

Future work should evaluate trends in exceedance frequencies of relative (percentile-based) heat stress thresholds. The absolute thresholds defined in Fig. 2b are applied on a national basis, meaning they may not be ideal for every location. Percentile-based thresholds can better distinguish changes in regional heat stress, for which acclimation is important (Fig. 2b; Grundstein et al. 2015; Rennie et al. 2021). In a review of heat-related mortality risk, Xu et al. (2016) found that extreme heat significantly affects mortality, but that the magnitude of these impacts vary with the definition of extreme heat, for which there is no universal definition (Perkins 2015). For example, heat-related mortality risks increased by 4% when heat waves were defined as mean temperatures ≥ the 95th percentile for ≥2 days but by 7% when defined as mean temperatures ≥ the 99th percentile for ≥2 days and 16% when defined as mean temperatures ≥ the 97th percentile for ≥5 days (Xu et al. 2016). Therefore, mortality is directly related to extreme heat intensity *and* duration, which any future percentile-based work should account for. Another related approach used in some epidemiology studies on heat stress is minimum mortality temperature (MMT), defined as the mean daily temperature at which the lowest mortality occurs (Folkerts et al. 2020). The MMT approach could be adapted for use with HI and WBGT and has particular utility in examining heat stress impacts on age groups (e.g., >65) or populations within a region that are vulnerable to the impacts of extreme heat (Folkerts et al. 2020).

Using station and reanalysis data, it will also be important to develop gridded climatologies of HI and WBGT for Florida, such as NCEI's nClimGrid (Vose et al. 2014) does for, for example, temperature. Furthermore, it should be quantified how much temperature and humidity changes have contributed to Florida summer heat stress trends. While temperature is generally (if unequally) increasing everywhere, humidity changes vary widely by latitude and region (e.g., Schoof et al. 2017). While warmer air can hold more water vapor, the subtropics are largely drying due to increased subsidence from the Hadley cell expansion (e.g., Rastogi et al. 2020). The Florida Peninsula, however, is unique in that it is surrounded by two large warm bodies of water. Therefore, the relative long-term contributions of temperature and humidity changes to summer heat stress trends are uncertain.

The physical processes that cause heat stress extremes should be investigated. While temperature advection is not always a large component of temperature extremes, moisture advection from nearby warm water can be important to humidity extremes (e.g., Rastogi et al. 2020). Furthermore, most temperature extremes are caused by a combination of subsidence (adiabatic warming) and surface sensible heat flux (diabatic warming). Latent heat flux, which is typically a mitigating factor for temperature extremes, can also increase humidity and therefore affect heat stress extremes. The relative importance of these processes to HI and WBGT extremes has not yet been quantified and should be a focus of future work.

Acknowledgments. This work was primarily supported by an Embry-Riddle Aeronautical University Faculty Innovative Research in Science and Technology (FIRST) Grant. The authors greatly thank North Carolina State Climatologist Dr. Kathie Dello, Jared Rennie of NOAA NCEI, and Darrian Bertrand of the Southern Climate Impacts Planning Program at the University of Oklahoma for their invaluable feedback and coding assistance throughout the project. We also acknowledge valuable conceptual discussions about WBGT with Philip Harvey of the U.S. military's Range Commanders Council Meteorology Group (RCC-MG) and Blaine Thomas of NOAA NWS (formerly of RCC-MG). Thanks are also given to the Iowa State University Iowa Environmental Mesonet (IEM) for making ISD data readily available in an easy-to-process format and to ECMWF for facilitating access to the ERA5 solar radiation data.

Data availability statement. Hourly HI is calculated using surface station data from the NOAA ISD (Smith et al. 2011). NOAA ISD is openly available from NOAA/NCEI (https://www.ncdc.noaa.gov/isd/data-access). Hourly WBGT is calculated using a combination of NOAA ISD and ERA5 hourly solar radiation data (Hersbach et al. 2020). ERA5 data are freely available at ECMWF's Climate Data Store (https://cds.climate.copernicus.eu/cdsapp#!/home), although a user account is required. The hourly HI and WBGT datasets produced in this study are available upon request by contacting the corresponding author.

REFERENCES

Brouillet, A., and S. Joussaume, 2019: Investigating the role of the relative humidity in the occurrence of temperature and heat stress extremes in CMIP5 projections. *Geophys. Res. Lett.*, **46**, 11 435–11 443, https://doi.org/10.1029/2019GL084156.

Budd, G. M., 2008: Wet-bulb globe temperature (WBGT)—Its history and its limitations. *J. Sci. Med. Sport*, **11**, 20–32, https://doi.org/10.1016/j.jsams.2007.07.003.

Carter, L., and Coauthors, 2018: Southeast. *Impacts, Risks, and Adaptation in the United States: Fourth National Climate Assessment*, D. R. Reidmiller et al., Eds., Vol. II, U.S. Global Change Research Program, 743–808, https://doi.org/10.7930/NCA4.2018.CH19.

Cloutier-Bisbee, S. R., A. Raghavendra, and S. M. Milrad, 2019: Heatwaves in Florida: Climatology, trends, and related precipitation events. *J. Appl. Meteor. Climatol.*, **58**, 447–466, https://doi.org/10.1175/JAMC-D-18-0165.1.

Diamond, H. J., and Coauthors, 2013: U.S. Climate Reference Network after one decade of operations. *Bull. Amer. Meteor. Soc.*, **94**, 485–498, https://doi.org/10.1175/BAMS-D-12-00170.1.

Diffenbaugh, N. S., and M. Ashfaq, 2010: Intensification of hot extremes in the United States. *Geophys. Res. Lett.*, **37**, L15701, https://doi.org/10.1029/2010GL043888.

Dimiceli, V. E., S. F. Piltz, and S. A. Amburn, 2013: Black globe temperature estimate for the WBGT Index. *IAENG Transactions on Engineering Technologies*, H. Kim, S. Ao, and B. Rieger, Eds., Springer, 323–334.

Di Napoli, C., F. Pappenberger, and H. L. Cloke, 2019: Verification of heat stress thresholds for a health-based heat-wave definition. *J. Appl. Meteor. Climatol.*, **58**, 1177–1194, https://doi.org/10.1175/JAMC-D-18-0246.1.

Easterling, D. R., and Coauthors, 2017: Precipitation change in the United States. *Climate Science Special Report: Fourth National Climate Assessment*, D. J. Wuebbles et al., Eds., Vol. I, U.S. Global Change Research Program, 207–230, https://doi.org/10.7930/J0H993CC.

Florida Department of Health, 2015: Health effects of summer heat in Florida. Accessed 28 May 2021, http://www.floridahealth.gov/environmental-health/climate-and-health/_documents/heat-profile.pdf.

Folkerts, M. A., P. Bröde, W. J. Wouter Botzen, M. L. Martinius, N. Gerrett, C. N. Harmsen, and H. A. M. Daanen, 2020: Long term adaptation to heat stress: Shifts in the minimum mortality temperature in the Netherlands. *Front. Physiol.*, **11**, 225, https://doi.org/10.3389/fphys.2020.00225.

Garland, R. M., M. Matooane, F. A. Engelbrecht, M.-J. M. Bopape, W. A. Landman, M. Naidoo, J. Van der Merwe, and C. Y. Wright, 2015: Regional projections of extreme apparent temperature days in Africa and the related potential risk to human health. *Int. J. Environ. Res. Public Health*, **12**, 12 577–12 604, https://doi.org/10.3390/ijerph121012577.

Greene, S., L. Kalkstein, D. Mills, and J. Samenow, 2011: An examination of climate change on extreme heat events and climate–mortality relationships in large U.S. cities. *Wea. Climate Soc.*, **3**, 281–292, https://doi.org/10.1175/WCAS-D-11-00055.1.

Grundstein, A., and J. Dowd, 2011: Trends in extreme apparent temperatures over the United States, 1949–2010. *J. Appl. Meteor. Climatol.*, **50**, 1650–1653, https://doi.org/10.1175/JAMC-D-11-063.1.

——, C. Williams, M. Phan, and E. Cooper, 2015: Regional heat safety thresholds for athletics in the contiguous United States. *Appl. Geogr.*, **56**, 55–60, https://doi.org/10.1016/j.apgeog.2014.10.014.

Habeeb, D., J. Vargo, and B. Stone Jr., 2015: Rising heat wave trends in large U.S. cities. *Nat. Hazards*, **76**, 1651–1665, https://doi.org/10.1007/s11069-014-1563-z.

Heo, S., M. L. Bell, and J.-T. Lee, 2019: Comparison of health risks by heat wave definition: Applicability of wet-bulb globe temperature for heat wave criteria. *Environ. Res.*, **168**, 158–170, https://doi.org/10.1016/j.envres.2018.09.032.

Herrera-Estrada, J. E., and J. Sheffield, 2017: Uncertainties in future projections of summer droughts and heat waves over the contiguous United States. *J. Climate*, **30**, 6225–6246, https://doi.org/10.1175/JCLI-D-16-0491.1.

Hersbach, H., and Coauthors, 2020: The ERA5 global reanalysis. *Quart. J. Roy. Meteor. Soc.*, **146**, 1999–2049, https://doi.org/10.1002/qj.3803.

Hussain, M. M., M. D. Manjurul, and I. Mahmud, 2019: pyMannKendall: A python package for non-parametric Mann Kendall family of trend tests. *J. Open Source Software*, **4**, 1556, https://doi.org/10.21105/joss.01556.

Keellings, D., and P. Waylen, 2014: Increased risk of heat waves in Florida: Characterizing changes in bivariate heat wave risk using extreme value analysis. *Appl. Geogr.*, **46**, 90–97, https://doi.org/10.1016/j.apgeog.2013.11.008.

——, and ——, 2015: Investigating teleconnection drivers of bivariate heat waves in Florida using extreme value analysis. *Climate Dyn.*, **44**, 3383–3391, https://doi.org/10.1007/s00382-014-2345-8.

——, and H. Moradkhani, 2020: Spatiotemporal evolution of heat wave severity and coverage across the United States. *Geophys. Res. Lett.*, **47**, e2020GL087097, https://doi.org/10.1029/2020GL087097.

Lemke, B., and T. Kjellstrom, 2012: Calculating workplace WBGT from meteorological data: A tool for climate change assessment. *Ind. Health*, **50**, 267–278, https://doi.org/10.2486/indhealth.MS1352.

Li, C., X. Zhang, F. Zwiers, Y. Fang, and A. M. Michalak, 2017: Recent very hot summers in Northern Hemispheric land areas measured by wet bulb globe temperature will be the norm within 20 years. *Earth's Future*, **5**, 1203–1216, https://doi.org/10.1002/2017EF000639.

Li, J., Y. D. Chen, T. Y. Gan, and N.-C. Lau, 2018: Elevated increased in human-perceived temperature under climate warming. *Nat. Climate Change*, **8**, 43–47, https://doi.org/10.1038/s41558-017-0036-2.

Liao, W., and Coauthors, 2018: Stronger contributions of urbanization to heat wave trends in wet climates. *Geophys. Res. Lett.*, **45**, 11 310–11 317, https://doi.org/10.1029/2018GL079679.

Liljegren, J. C., R. A. Carhart, P. Lawday, S. Tschopp, and R. Sharp, 2008: Modeling the wet bulb globe temperature using standard meteorological measurements. *J. Occup. Environ. Hyg.*, **5**, 645–655, https://doi.org/10.1080/15459620802310770.

Limaye, V. S., J. Vargo, M. Harkey, T. Holloway, and J. A. Patz, 2018: Climate change and heat-related excess mortality in the eastern USA. *EcoHealth*, **15**, 485–496, https://doi.org/10.1007/s10393-018-1363-0.

Little, C. M., R. M. Horton, R. E. Kopp, M. Oppenheimer, G. A. Vecchi, and G. Villarini, 2015: Joint projections of U.S. East Coast sea level and storm surge. *Nat. Climate Change*, **5**, 1114–1120, https://doi.org/10.1038/nclimate2801.

McGregor, G., and J. Vanos, 2018: Heat: A primer for public health researchers. *Public Health*, **161**, 138–146, https://doi.org/10.1016/j.puhe.2017.11.005.

Meehl, G. A., J. M. Arblaster, and G. Branstator, 2012: Mechanisms contributing to the warming hole and the consequent U.S. east–west differential of heat extremes. *J. Climate*, **25**, 6394–6408, https://doi.org/10.1175/JCLI-D-11-00655.1.

Mora, C., and Coauthors, 2017: Global risk of deadly heat. *Nat. Climate Change*, **7**, 501–506, https://doi.org/10.1038/nclimate3322.

Newth, D., and D. Gunasekera, 2018: Projected changes in wet-bulb globe temperature under alternative climate scenarios. *Atmosphere*, **9**, 187, https://doi.org/10.3390/atmos9050187.

Nissan, H., K. Burkart, E. C. de Perez, M. Van Aalst, and S. Mason, 2017: Defining and predicting heat waves in Bangladesh.

J. Appl. Meteor. Climatol., **56**, 2653–2670, https://doi.org/10.1175/JAMC-D-17-0035.1.

NWS New York, 2021: Excessive heat page. Accessed 24 May 2021, https://www.weather.gov/okx/excessiveheat.

Oklahoma Mesonet, 2016: Wet bulb globe temperature category work/rest and water intake. Accessed 24 May 2021, http://www.mesonet.org/images/site/WBGT_Mesonet_Work_Rest_Info.May2016.pdf.

Oleson, K. W., A. Monaghan, O. Wilhelmi, M. Barlage, N. Brunsell, J. Feddema, L. Hu, and D. F. Steinhoff, 2015: Interactions between urbanization, heat stress, and climate change. *Climatic Change*, **129**, 525–541, https://doi.org/10.1007/s10584-013-0936-8.

Ono, M., and M. Tonouchi, 2014: Estimation of wet-bulb globe temperature using generally measured meteorological indices. *Japan Soc. Biometeor.*, **50**, 147–157, https://doi.org/10.11227/seikisho.50.147.

Ortiz, L. E., and J. E. Gonzalez, 2018: New York City impacts on a regional heat wave. *J. Appl. Meteor. Climatol.*, **57**, 837–851, https://doi.org/10.1175/JAMC-D-17-0125.1.

Partridge, T. F., J. M. Winter, E. C. Osterberg, D. W. Hyndman, A. D. Kendall, and F. J. Magilligan, 2018: Spatially distinct seasonal patterns and forcings of the U.S. warming hole. *Geophys. Res. Lett.*, **45**, 2055–2063, https://doi.org/10.1002/2017GL076463.

Perkins, S. E., 2015: A review on the scientific understanding of heat waves—Their measurement, driving mechanisms, and changes at the global scale. *Atmos. Res.*, **164–165**, 242–267, https://doi.org/10.1016/j.atmosres.2015.05.014.

——, L. V. Alexander, and J. R. Nairn, 2012: Increasing frequency, intensity, and duration of observed global heat waves and warm spells. *Geophys. Res. Lett.*, **39**, 2012GL053361, https://doi.org/10.1029/2012GL053361.

Raghavendra, A., A. Dai, S. M. Milrad, and S. R. Cloutier-Bisbee, 2019: Floridian heatwaves and extreme precipitation: Future climate projections. *Climate Dyn.*, **52**, 495–508, https://doi.org/10.1007/s00382-018-4148-9.

Ramamurthy, P., and E. Bou-Zeid, 2017: Heat waves and urban heat islands: A comparative analysis of multiple cities. *J. Geophys. Res. Atmos.*, **122**, 168–178, https://doi.org/10.1002/2016JD025357.

Rastogi, D., F. Lehner, and M. Ashfaq, 2020: Revisiting recent U.S. heat waves in a warmer and more humid climate. *Geophys. Res. Lett.*, **47**, https://doi.org/10.1029/2019GL086736.

Raymond, C., D. Singh, and R. M. Horton, 2017: Spatiotemporal patterns and synoptics of extreme wet-bulb temperature in the contiguous United States. *J. Geophys. Res. Atmos.*, **122**, 13 108–13 124, https://doi.org/10.1002/2017JD027140.

——, T. Matthews, and R. M. Horton, 2020: The emergence of heat and humidity too severe for human tolerance. *Sci. Adv.*, **6**, eaaw1838, https://doi.org/10.1126/sciadv.aaw1838.

Rennie, J., J. E. Bell, K. E. Kunkel, S. Herring, H. Cullen, and A. M. Abadi, 2019: Development of a submonthly temperature product to monitor near-real-time climate conditions and assess long-term heat events in the United States. *J. Appl. Meteor. Climatol.*, **58**, 2653–2674, https://doi.org/10.1175/JAMC-D-19-0076.1.

——, M. A. Palecki, S. P. Heuser, and H. J. Diamond, 2021: Developing and validating heat exposure products using the U.S. Climate Reference Network. *J. Appl. Meteor. Climatol.*, **60**, 543–558, https://doi.org/10.1175/JAMC-D-20-0282.1.

Rogers, J. C., 2013: The 20th century cooling trend over the southeastern United States. *Climate Dyn.*, **40**, 341–352, https://doi.org/10.1007/s00382-012-1437-6.

Rothfusz, L. P., 1990: The heat index "equation" (or, more than you ever wanted to know about heat index). NWS Southern Region Headquarters Tech. Attachment SR-90-23, 2 pp., https://www.weather.gov/media/ffc/ta_htindx.PDF.

Schoof, J. T., T. W. Ford, and S. C. Pryor, 2017: Recent changes in U.S. regional heat wave characteristics in observations and reanalyses. *J. Appl. Meteor. Climatol.*, **56**, 2621–2636, https://doi.org/10.1175/JAMC-D-16-0393.1.

Shiva, J. S., D. G. Chandler, and K. E. Kunkel, 2019: Localized changes in heat wave properties across the United States. *Earth's Future*, **7**, 300–319, https://doi.org/10.1029/2018EF001085.

Smith, A., N. Lott, and R. Vose, 2011: The Integrated Surface Database: Recent developments and partnerships. *Bull. Amer. Meteor. Soc.*, **92**, 704–708, https://doi.org/10.1175/2011BAMS3015.1.

Smith, T. T., B. F. Zaitchik, and J. M. Gohlke, 2013: Heat waves in the United States: Definitions, patterns, and trends. *Climatic Change*, **118**, 811–825, https://doi.org/10.1007/s10584-012-0659-2.

Steadman, R. G., 1984: A universal scale of apparent temperature. *J. Climate Appl. Meteor.*, **23**, 1674–1687, https://doi.org/10.1175/1520-0450(1984)023<1674:AUSOAT>2.0.CO;2.

Stull, R. S., 2011: Wet-bulb temperature from relative humidity and air temperature. *J. Appl. Meteor. Climatol.*, **50**, 2267–2269, https://doi.org/10.1175/JAMC-D-11-0143.1.

Takakura, J., S. Fujimori, K. Takahashi, Y. Hijioka, and Y. Honda, 2019: Site-specific hourly resolution wet bulb globe temperature reconstruction from gridded daily resolution climate variables for planning climate change adaptation measures. *Int. J. Biometeor.*, **63**, 787–800, https://doi.org/10.1007/s00484-019-01692-3.

Taylor, M. A., and L. A. Clarke, 2018: Future Caribbean climates in a world of rising temperatures: The 1.5 vs. 2.0 dilemma. *J. Climate*, **31**, 2907–2926, https://doi.org/10.1175/JCLI-D-17-0074.1.

Vose, R. S., and Coauthors, 2014: Improved historical temperature and precipitation time series for U.S. climate divisions. *J. Appl. Meteor. Climatol.*, **53**, 1232–1251, https://doi.org/10.1175/JAMC-D-13-0248.1.

Weatherly, J. W., and M. A. Rosenbaum, 2017: Future projections of heat and fire-risk indices for the contiguous United States. *J. Appl. Meteor. Climatol.*, **56**, 863–876, https://doi.org/10.1175/JAMC-D-16-0068.1.

Weinberger, K. R., D. Harris, K. R. Spangler, A. Zanobetti, and G. A. Wellenius, 2020: Estimating the number of excess deaths attributable to heat in 297 United States counties. *Environ. Epidemiol.*, **4**, e096, https://doi.org/10.1097/EE9.0000000000000096.

Willett, K. M., and S. Sherwood, 2012: Exceedance of heat index thresholds for 15 regions under a warming climate using the wet-bulb globe temperature. *Int. J. Climatol.*, **32**, 161–177, https://doi.org/10.1002/joc.2257.

Wouters, H., and Coauthors, 2017: Heat stress increase under climate change twice as large in cities as in rural areas: A study for a densely populated midlatitude maritime region. *Geophys. Res. Lett.*, **44**, 8997–9007, https://doi.org/10.1002/2017GL074889.

Xu, Z., G. FitzGerald, Y. Guo, B. Jalaludin, and S. Tong, 2016: Impact of heatwave on mortality under different heatwave definitions: A systematic review and meta-analysis. *Environ. Int.*, **89–90**, 193–203, https://doi.org/10.1016/j.envint.2016.02.007.

CORRIGENDUM

CAITLYN MCALLISTER,[a] AARON STEPHENS,[a] AND SHAWN M. MILRAD[a]

[a] *Meteorology Program, Applied Aviation Sciences Department, Embry-Riddle Aeronautical University, Daytona Beach, Florida*

(Manuscript received 17 August 2022, in final form 30 September 2022)

The wet-bulb globe temperature (WBGT) calculation code that we used for our published article (McAllister et al. 2022) had a previously undiscovered temperature unit error in it, resulting in our original WBGT calculations being too low. This affected Figs. 5, 6, and 9, as well as Tables 3 and 5, for all of which we present corrected versions here. In general, the corrections make our trend analyses and results more robust and demonstrate that heat stress increases in Florida are even more profound than McAllister et al. (2022) originally showed. The results for heat index in McAllister et al. (2022) are completely unaffected.

The changes to Figs. 5 and 6 and Table 3 (WBGT trends) are relatively minor and primarily affect WBGT magnitudes, which were previously underestimated. The trends and conclusions discussed in section 3b of McAllister et al. (2022) are largely unchanged, with the following notable exceptions:

- Increases in daily maximum WBGT are now statistically significant (Mann–Kendall test; Table 3) at six of eight cities [the exceptions are Pensacola (KPNS) and Key West (KEYW)]. In McAllister et al. (2022), only four of eight cities exhibited statistically significant increases.
- Period differences in maximum WBGT are statistically significant at five of eight cities, excluding KPNS, Jacksonville (KJAX), and KEYW (Table 3). In McAllister et al. (2022), statistically significant differences were found at six of eight stations (the exceptions were KPNS and KJAX).
- Statistically significant increases and period differences in daily mean and minimum WBGT remain true across the board, with the minor exception of period differences in daily mean WBGT at Orlando (KMCO). The daily mean WBGT period difference is still positive (Table 3) but is now not statistically significant.
- Particularly since 2000, all eight cities feature average summer daily maximum WBGT substantially greater than 90°F (Figs. 5, 6), considered to be "extreme" by the U.S. Occupational Safety and Health Administration. In McAllister et al. (2022), a few cities had values slightly less than 90°F.

Because our previous code underestimated WBGT magnitudes by approximately 2°–3°F, the changes to Fig. 9 and Table 5 (WBGT threshold exceedance frequencies) are substantial. As such, we strongly encourage the reader to refer to the following discussion instead of the threshold frequency analysis contained in parts of sections 4b and 5 in McAllister et al. (2022).

Figure 9 shows the number of summer days per year in which each daily maximum WBGT absolute threshold (moderate, high, and extreme) is exceeded. Corresponding trends and significance test results are shown in Table 5. High WBGT summer days exhibit statistically significant frequency at all eight cities (Table 5). Extreme WBGT days also increase at all eight locations, but the increases are only statistically significant at six cities (the exceptions are KPNS and KMCO). Furthermore, moderate WBGT days decrease in frequency at all eight cities (Table 5; Fig. 9), and significantly so at five of eight locations (the exceptions are KPNS, KJAX, and KMCO). Trends across Florida are marked by formerly moderate WBGT days being replaced by high and extreme WBGT days, emphasizing an alarming increase in hazardous heat stress.

The largest statistically significant positive frequency trends in high WBGT days occur at Miami (KMIA; 0.344 days yr^{-1}), Daytona Beach (KDAB; 0.333 days yr^{-1}), and Tampa (KTPA; 0.308 days yr^{-1}), corresponding to the largest positive trends in daily maximum WBGT (Figs. 5, 6; Table 3). For extreme

Corresponding author: Shawn M. Milrad, milrads@erau.edu

DOI: 10.1175/JAMC-D-22-0130.1

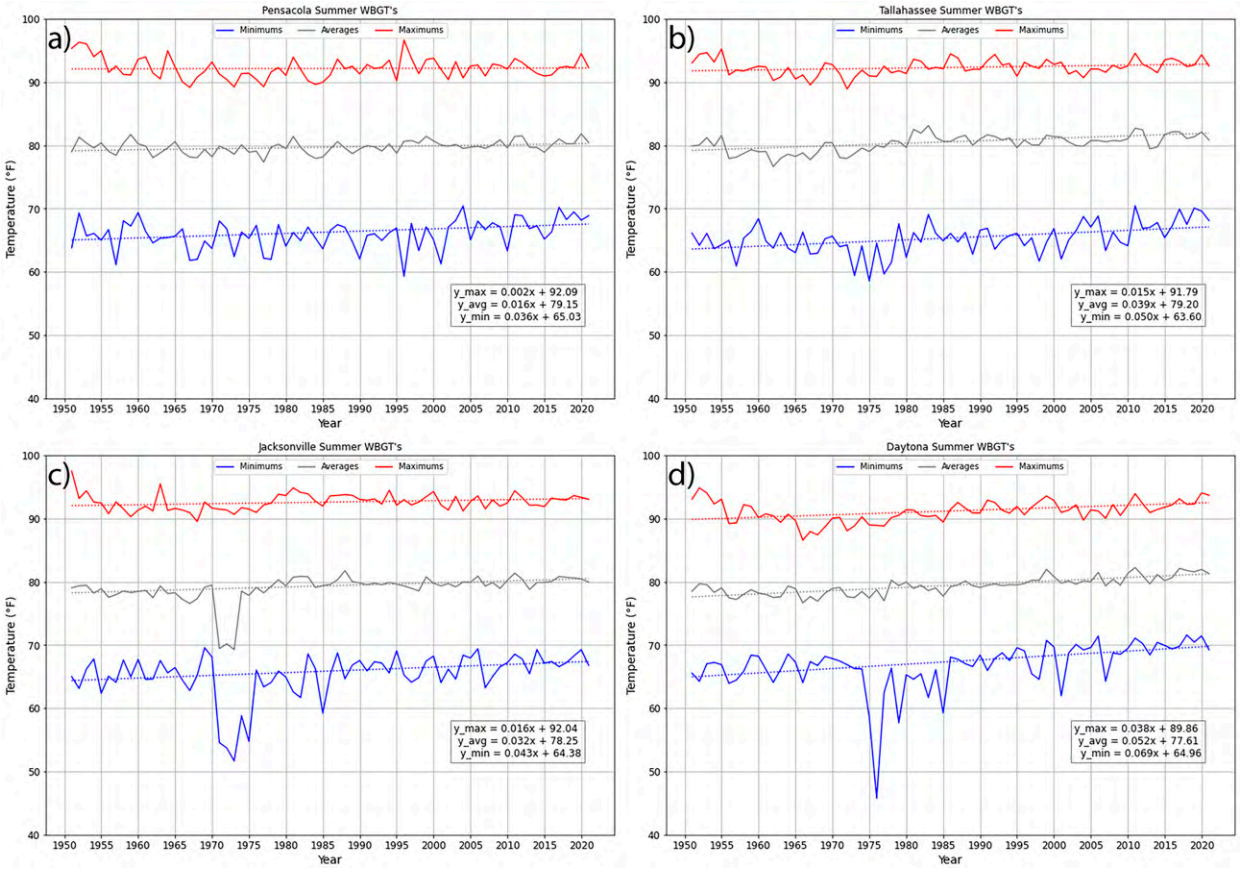

FIG. 5. Observations and linear trends in average summer [June–August (JJA)] daily maximum (red), mean (gray), and minimum (blue) WBGT (1950–2020) at (a) KPNS, (b) Tallahassee (KTLH), (c) KJAX, and (d) KDAB. Linear trend lines (dashed) for each variable are based on the Theil–Sen estimator, with the corresponding values (°F yr^{-1}) displayed in Table 3. The Z scores and p values of trends based on the MK significance test, as well as p values from the Student's t test evaluating differences between the first (1950–84) and last (1986–2020) 35 years in the study period, are also shown in Table 3. Trends (MK) and period differences (Student's t test) are deemed statistically significant when $p \leq 0.05$.

WBGT day increases, KEYW and KJAX rank second and third, respectively, after KDAB, followed by KTPA and KMIA (Table 5). These results demonstrate that increases in high and extreme WBGT days are most prominent at coastal locations in the Florida Peninsula and Florida Keys. Given the documented increase in SSTs and associated evaporation/humidity in coastal subtropical locations over the past few decades (e.g., Little et al. 2015; Raymond et al. 2020), this is likely not a coincidence.

Overall, WBGT threshold frequency trends (Fig. 9; Table 5) show a substantial escalation in hazardous heat stress during Florida summers. Particularly since 2000, most stations are experiencing >30 high and >20 extreme WBGT days per summer (Fig. 9), meaning that more than one-half of summer days pose a large threat to human health, especially for outdoor workers (e.g., agricultural and construction) and individuals without access to sufficient cooling systems.

The authors greatly apologize for the WBGT coding error ("bug") that we did not discover sooner and that necessitated this corrigendum.

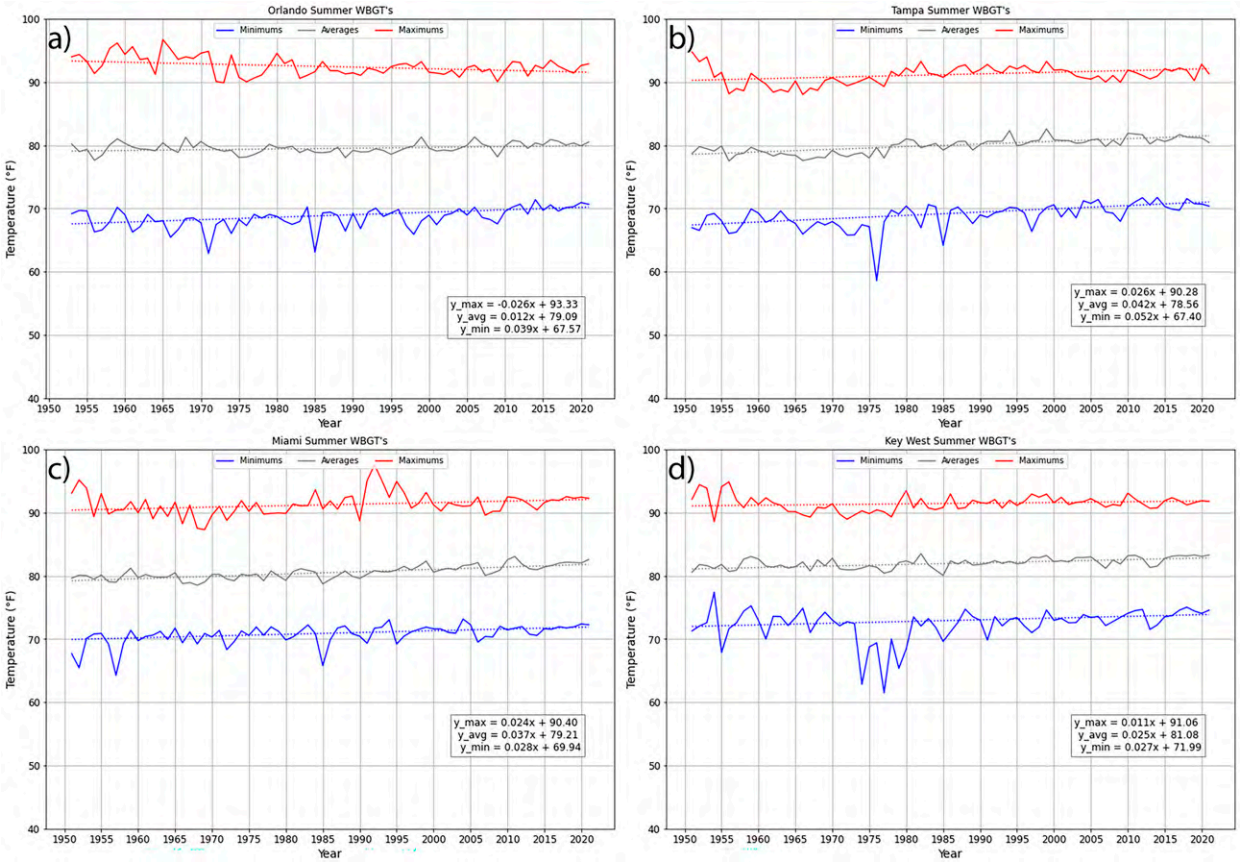

FIG. 6. As in Fig. 5, but for (a) KMCO, (b) KTPA, (c) KMIA, and (d) KEYW. Corresponding statistics are shown in Table 3. Note that all stations except KMCO start in 1950; KMCO data start in 1952 (Table 1 of McAllister et al. 2022).

REFERENCES

Little, C. M., R. M. Horton, R. E. Kopp, M. Oppenheimer, G. A. Vecchi, and G. Villarini, 2015: Joint projections of U.S. East Coast sea level and storm surge. *Nat. Climate Change*, **5**, 1114–1120, https://doi.org/10.1038/nclimate2801.

McAllister, C., A. Stephens, and S. M. Milrad, 2022: The heat is on: Observations and trends of heat stress metrics during Florida summers. *J. Appl. Meteor. Climatol.*, **61**, 277–296, https://doi.org/10.1175/JAMC-D-21-0113.1.

Raymond, C., T. Matthews, and R. M. Horton, 2020: The emergence of heat and humidity too severe for human tolerance. *Sci. Adv.*, **6**, eaaw1838, https://doi.org/10.1126/sciadv.aaw1838.

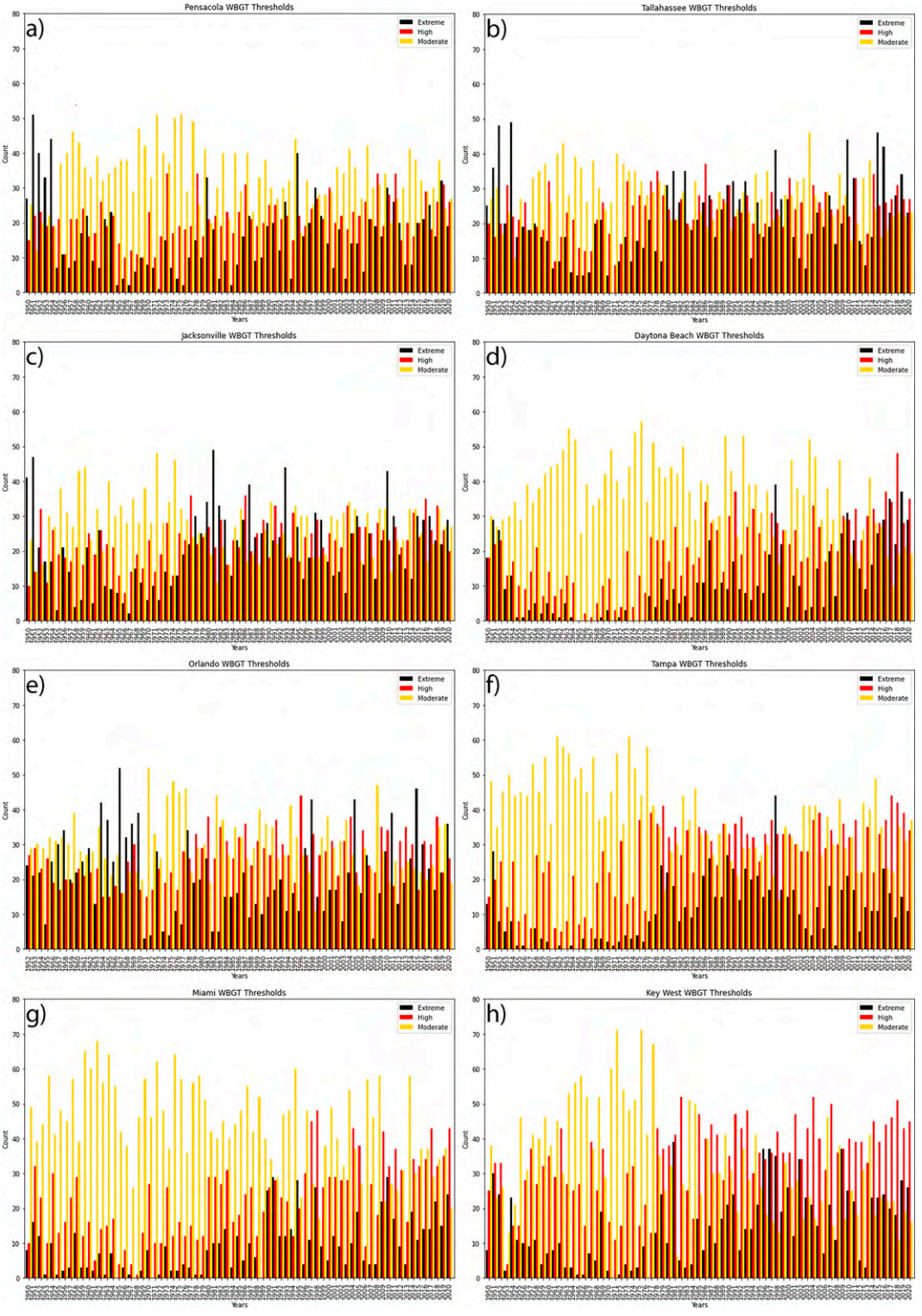

FIG. 9. Frequency histograms (days yr^{-1}) of summer (JJA) daily maximum WBGT that fit the moderate (yellow), high (red), and extreme (black) threshold categories defined in Fig 2b of McAllister et al. (2022). Corresponding statistics are shown in Table 5. Shown here are (a) KPNS, (b) KTLH, (c) KJAX, (d) KDAB, (e) KMCO, (f) KTPA, (g) KMIA, and (h) KEYW. All histograms are for 1950–2020, except for KMCO (1952–2020).

TABLE 3. As in Table 2 of McAllister et al. (2022), but for the average summer daily WBGT observations and trends (1950–2020) displayed in Figs. 5 and 6.

	Trend (°F yr^{-1})	Z score (MK)	p value (MK)	p value (t test)
KPNS				
Max	0.002	0.109	0.913	0.199
Mean	0.016	2.770	0.006	0.001
Min	0.036	2.780	0.005	0.049
KTLH				
Max	0.015	1.985	0.047	0.044
Mean	0.039	4.954	7.281×10^{-7}	7.273×10^{-6}
Min	0.050	3.852	1.172×10^{-4}	0.001
KJAX				
Max	0.016	2.055	0.040	0.095
Mean	0.032	5.361	8.289×10^{-8}	1.766×10^{-4}
Min	0.043	3.200	0.001	1.668×10^{-4}
KDAB				
Max	0.034	3.733	1.894×10^{-4}	2.475×10^{-5}
Mean	Max	7.333	2.196×10^{-13}	3.548×10^{-13}
Min	Mean	5.252	1.508×10^{-7}	1.370×10^{-5}
KMCO				
Max	−0.026	−2.440	0.015	0.003
Mean	0.012	2.429	0.015	0.120
Min	0.039	4.366	1.264×10^{-5}	4.096×10^{-4}
KTPA				
Max	0.026	2.988	0.003	7.407×10^{-4}
Mean	0.042	6.890	5.598×10^{-12}	8.157×10^{-14}
Min	0.052	5.539	3.035×10^{-8}	2.057×10^{-6}
KMIA				
Max	0.024	2.392	0.017	0.003
Mean	0.037	6.969	3.193×10^{-12}	6.311×10^{-11}
Min	0.028	4.606	4.100×10^{-6}	1.739×10^{-4}
KEYW				
Max	0.011	1.439	0.150	0.098
Mean	0.025	5.033	4.826×10^{-7}	1.684×10^{-6}
Min	0.027	2.809	0.005	0.003

TABLE 5. Statistics for the average summer daily maximum WBGT threshold category trends shown in Fig. 9. From left to right: threshold category [Fig 2b of McAllister et al. (2022)] and number n of events in each category throughout the climatology period, linear trends (days yr^{-1}) using the Theil–Sen estimator, and Z scores and p values of the linear trends from the MK significance test. Results are considered to be statistically significant when $p \leq 0.05$ (marked in ***boldface italics***).

Category	Trend (days yr^{-1})	Z score (MK)	p value (MK)
KPNS			
Moderate (n = 2357)	−0.063	−1.133	0.257
High (n = 1494)	0.098	2.973	***0.003***
Extreme (n = 1129)	0.103	1.491	0.136
KTLH			
Moderate (n = 1971)	−0.091	−2.028	***0.042***
High (n = 1671)	0.104	2.735	***0.006***
Extreme (n = 1500)	0.135	2.067	***0.039***
KJAX			
Moderate (n = 1931)	−0.059	−1.313	0.189
High (n = 1633)	0.143	4.010	$\boldsymbol{6.083 \times 10^{-5}}$
Extreme (n = 1475)	0.170	2.773	***0.006***
KDAB			
Moderate (n = 2560)	−0.186	−2.868	***0.004***
High (n = 1437)	0.333	6.054	$\boldsymbol{1.416 \times 10^{-9}}$
Extreme (n = 768)	0.250	4.577	$\boldsymbol{4.728 \times 10^{-6}}$
KMCO			
Moderate (n = 2055)	−0.080	−1.749	0.080
High (n = 1811)	0.154	3.601	$\boldsymbol{3.164 \times 10^{-9}}$
Extreme (n = 1462)	0	0.140	0.889
KTPA			
Moderate (n = 2723)	−0.295	−4.592	$\boldsymbol{4.398 \times 10^{-6}}$
High (n = 1908)	0.308	5.484	$\boldsymbol{4.166 \times 10^{-8}}$
Extreme (n = 782)	0.158	3.216	***0.001***
KMIA			
Moderate (n = 3118)	−0.286	−3.393	$\boldsymbol{8.315 \times 10^{-8}}$
High (n = 1617)	0.344	5.328	$\boldsymbol{9.920 \times 10^{-8}}$
Extreme (n = 646)	0.156	4.341	$\boldsymbol{1.420 \times 10^{-5}}$
KEYW			
Moderate (n = 2386)	−0.355	−4.277	$\boldsymbol{1.896 \times 10^{-5}}$
High (n = 2414)	0.287	5.044	$\boldsymbol{4.552 \times 10^{-7}}$
Extreme (n = 1036)	0.243	3.848	$\boldsymbol{1.191 \times 10^{-4}}$